Satellite Based Flood Forecasting for the Koshi River Basin, Nepal

by

Md. Kamrul Hossain

A thesis progress report submitted in partial fulfillment of the requirements for the degree of Master of Engineering in
Water Engineering & Management

Examination Committee:	Prof. Mukand S Babel (Chairperson) Dr. Sangam Shrestha Dr. Sarawut Ninsawat Dr. Shahriar Wahid

Nationality:	Bangladeshi
Previous Degree:	Bachelor of Engineering in Civil Engineering, Bangladesh University of Engineering & Technology Dhaka, Bangladesh
Scholarship Donor:	ADB-JSP

Asian Institute of Technology
School of Engineering and Technology
Thailand
April, 2014

ACKNOWLEDGEMENTS

Foremost, I would like to express my sincere gratitude to my advisor Prof. Mukand S Babel for the continuous support of my master study and research, for his patience, motivation, enthusiasm, and immense knowledge. His guidance helped me in all the time of research and writing of this thesis. I could not have imagined having a better advisor and mentor for my master study.

Besides my advisor, I would like to thank the rest of my thesis committee: Dr. Sangam Shrestha, Dr. Sarawut Ninsawat and Dr. Shahriar Wahid, for their encouragement, insightful comments, and hard questions.

It has been a pleasure and honor for me, to complete my master thesis under the Asian Development Bank (ADB) - Japan Scholarship Program (JSP) scholarship, I should not forget to thank the Asian Development Bank (ADB) for their financial support throughout my master degree including the thesis period and their trust towards me and my capability. Special thanks are due for the research support provided by the Koshi Basin Programme, Phase I (KBP) - funded by the Department of Foreign Affairs and Trade (DFAT), Australian Government and implemented by the International Centre for Integrated Mountain Development (ICIMOD), Nepal.

My sincere thanks also goes to Mr. Abu Saleh Khan, Mr. Sardar Mohammad Shah-Newaz and Mr. Tanvir Ahmed, for giving me the opportunity and valuable advises in Institute of Water Modelling (IWM) for model development purpose.

I thank Mr. Pradeep Dangol and Dr. Santosh Nepal at ICIMOD, Mr. Fakhruddin Bapon, Mr. Anshul Agarwal and Dr. Faisal Hossain for enlightening me the first glance of research.

Last but not the least, I would like to thank my family: my parents Mr. Md Delwar Hossain and Mrs. Roushan ara Begum, for giving birth to me at the first place and supporting me spiritually throughout my life.

ABSTRACT

Flood became more frequent and devastating disaster in recent world. Flood forecasting is an essential tool for flood mitigation strategies. The Koshi River is one of the major tributaries of the Ganges. Before joining the Ganges River, almost every year it floods the downstream areas. As upstream area in Himalayan range, hydro-meteorological data is very scarce in that region. Using remote sensing technology to abstract hydro-meteorological data is possible to acquire and this technology is emerging day by day. The Koshi River has a number of tributaries and all of them have originated from Himalayan range. This river basin has high elevation difference. High elevated upstream region prevails an arctic climate whereas low elevated downstream region exhibits tropical climate. Glacier are a common feature in the upstream area.

To develop flood forecasting model, data acquisition was done from different sources. To estimate flow in real time, a technique was developed using passive microwave AMSR-E image. This technique exhibits about 75% correlation between simulated and observed flow with 0.0092 m/km ground slope or lower. Above this slope this microwave AMSR-E approach technique does not show acceptable correlation, because that region is denoted as mountainous region. Rivers in mountainous region are comparatively narrow and there is no flood plain. To overcome this problem, another technique was developed using water surface reflectance of LANDSAT imagery. The principle of water surface reflectance approach for remote flow estimation is the attenuation attribute of spectrum in water. This attenuation attribute can be correlate with observed flow. LANDSAT images are not available in daily basis and also interfered by cloud cover in monsoon. Simulated data shows acceptable error with observed flow. Comparison among observed flow, estimated flow and flow from NAM model was performed and results shows acceptable correlation.

Hydrological model was development using Aphrodite rainfall appears more suitable for flood forecasting. To acquire recent temperature and evaporation data, MODIS LST and temperature vs evaporation correlation was used respectively. Data acquisition for hydrodynamic model was done using DHM flow data and DEM data. As no historical water level information was not available, flow forecasting was performed. Using GFS or ECMWF rainfall forecast, flow forecasting exhibits random results. Using pre-monsoon and monsoon flow to test the FF model shows that, flow forecast is in acceptable limit upto 2-4 day. After 4 days flow forecast has high error. This FF model is has capability to work with recent dataset and forecast in real time.

TABLE OF CONTENTS

LIST OF FIGURES

TITLE **PAGE**

LIST OF TABLES

TITLE **PAGE**

LIST OF ABBREVIATIONS

AMSR-E	Advanced Microwave Scanning Radiometer - Earth Observing System
ASTER	Advanced Space-borne Thermal Emission and Reflection Radiometer
CC	Climate Change
CMS	Cubic Meter per Second
DEM	Digital Elevation Model
DHM	Department of Hydrology Meteorology
DN	Digital Numbers
ECMWF	European Centre for Medium Range Weather Forecasts
ETM+	Enhanced Thematic Mapper Plus
FF	Flood Forecasting
GFS	Global Forecast System
GLOF	Glacier Lake Outburst Flood
GMS	Geostationary Meteorological Satellite
HD	Hydro Dynamic
ICIMOD	International Centre for Integrated Mountain Development
IPCC	Inter-governmental Panel on Climate Change
IR	Infra-Red
JAXA	Japan Aerospace Exploration Agency
LST	Land Surface Temperature
MCM	Million Cubic Meter
MODIS	Moderate-Resolution Imaging Spectroradiometer
NAM	Nedbør Afstrømnings Model
NASA	National Aeronautics and Space Administration
NCEP	National Center for Environmental Prediction
OLI	Operational Land Imager
SAR	Synthetic Aperture Radar
SLR	Sea Level Rise
SRM	Snowmelt Runoff Model
SRTM	Shuttle Radar Topography Mission
TOVAS	TRMM Online Visualization and Analysis System
TIRS	Thermal Infrared Sensor
TRMM	Tropical Rainfall Measuring Mission
TOF	Time of Forecast
WMO	World Meteorological Organization
WRF	Weather Research and Forecasting

CHAPTER 1
INTRODUCTION

1.1 BACKGROUND

Flooding is an ever known common calamity in water resources sector. According to WMO, flood is defined as rise in stream water level to a peak from which the water level recedes at a slower rate. It is also known as relatively high flow measured by stage height, discharge and rising tide. Flood has occupied 50% of total water related natural disaster and rest of the causes are landslide, famine, water related epidemic, drought etc. Seasonal monsoon rainfall often cause flood in south-Asia. Unplanned flood protection, land use, pollution also cause flood. Flood often carries a huge amount of sediments which ultimately settles in river bed and lessens the conveyance capacity of the river which causes flood. Main damage of flooding include loss of life, damage of infrastructure and contamination of potable water. **Figure 1.1** shows increasing trend of flood occurrence from last century. China has faced the most devastated flood ever in history in 1931 where nearly 3.7 to 4 million people died. South Asia is a flood prone region due to heavy monsoon rainfall, huge sedimentation load from upstream and increasing human interventions.

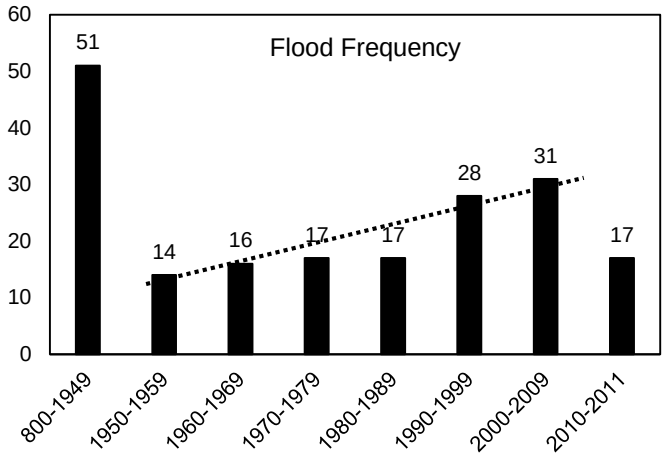

Figure 1.1: Worldwide flood frequency

Flood forecasting is a necessary part of flood Management. Provision of flood forecasting will form part of flood management planning and development strategies. A remote-sensing-based flow measurement technique for rivers is emerging. High-resolution hydro-meteorological imagery was used to forecast the flash flood in Venice in 2007 (Rossa et al., 2010) This phenomena opens a door of wide scope for surface water data collection, accuracy evaluation and results dissemination without regard to political boundaries. It also opens a horizon to acquire data in inaccessible area and develop the capacity to hydrological and hydro-dynamic analysis.

Remote sensed hydro-meteorological measurement has merits and demerits. Satellite data has benefit of wide coverage of area, latest authentic information, unbound by political boundaries, easy accessibility. But sometimes satellite images are in coarse resolution with less accuracy. Satellite imagery has application to monitor drought, determine hydrologic characterization of snowpack, investigate soil moisture, energy flux, roughness and refractivity of sea ice etc. (Zhang & Jia, 2013; Li, Durand & Margulis, 2012; Lu et al., 2012; Hong, 2010; Cashion, Lakshmi, Bosch & Jackson, 2005).

1.2 STATEMENT OF THE PROBLEM

The Koshi River is highly flood prone river. It is a tributary of a major river like the Ganges and the Koshi River itself is a huge river. This river carries snowmelt runoff from Mt. Everest, Mt. Kanchenjunga, Mt. Gosainthan and other premier mountain peaks. Moreover it has comparatively high capacity of sediment transport. This river collect sediments from mountains and when it travels through flat slope in downstream it deposited a huge amount of sediment. This sedimentation cause frequent flooding as well as course movement.

Flood forecasting in this region carries huge interest, because this river basin is home of millions of people. The Koshi River comes from Himalayan range, passing through Bihar India and joins with the Ganges. In the Monsoon season, the Koshi River contains huge amount of water and floods the flat terrain in its downstream. This flood incident is also influenced by high sediment yield of the river.

Hydro meteorological instrument in the Himalayan mountain area is scarce, because of inaccessibility. But this upstream region is important in a sense of that it is responsible to contribute inflow via snow melt and rainfall to downstream rivers. Using satellite imagery to estimate hydrologic and hydraulic parameters is a state of art method which has a high potential to enrich the data availability in this mountainous area.

Flood forecasting for the Koshi River will help to develop an effective flood warning system for the downstream area. It will help to reduce the loss of life, damage of infrastructure and crops. Flood forecasting will also help to develop an effective flood mitigation strategy. Assessment of the flood protection work can be done and appropriate measures can be taken for upcoming extreme events.

1.3 OBJECTIVE

The main objective of this research is to forecast flood for the Terai region of the Koshi River Basin using satellite imagery. To achieve this objective following sub-objectives are required to be achieved:

- To estimate upstream river flow using satellite imagery and remote sensing.
- To develop a flow forecasting model and accuracy analysis.
- To forecast and analyze the effect of flow in the study basin.

1.4 SCOPE OF THE STUDY

- Review and compilation of historic climatic and hydro-meteorological data including extreme events considering spatial and temporal distribution.
- Acquisition of satellite imagery and data extraction, preparation, processing.
- Correlation of Satellite derived data and actual data from a known location.

- Appropriate correction for hydro-meteorological data.
- Development of hydrological (NAM) model and hydrodynamic (HD) of the Koshi basin.
- Calibration and validation of the models using available historical observed data.
- Development of flood forecasting (FF) model of the Koshi basin.
- Acquisition of rainfall forecast data from different sources.
- Use of flood forecasting model to forecast historical extreme event and accuracy analysis.
- Applicability of flood forecasting model for current use and real-time forecasting.

1.5 LIMITATIONS OF THE STUDY

- Due to unavailability of LANDSAT daily data, time series generation is not possible using remote flow estimation technique.
- This study is limited to flow forecasting due to unavailability of historical water level data.
- Due to unavailability of temperature recording station in Himalayan region, grid based observed temperature is the only source of data.
- The amount of error is relatively high for satellite based rainfall. Forecasting flood based on satellite extracted rainfall thus contain comparatively high error.

CHAPTER 2
LITERATURE REVIEW

2.1 HYDRO-METEOROLOGICAL MEASUREMENT

Hydro-meteorological measurement includes hydrological measurement i.e. water level, discharge, water quality, erosion, sedimentation etc. and meteorological measurement i.e. temperature, evaporation, water vapor etc. For this research, it is imperative to concentrate on discharge measurement. Discharge measurement is associated with classical mechanical measurement using current meter, pelton wheel, Woltmann meter, jet meter, turbine flow meter etc. or pressure based meter using venture meter, orifice plate, pressure probe etc. or open channel flow measurement using dye, area-velocity, acoustic Doppler etc. All this measurement requires physical contact with flow which appears relatively difficult for inaccessible places. To overcome this problem flow measurement using remote sensing and telemetric network is emerging. This technologies also have an advantage to real time data acquisition. Brakenridge et al. (2007) used microwave AMSR-E images to estimate river flow in different stations globally. Hossain et.al. (2013) used altimetry data to estimate river flow. Stumpf et al. (2003) developed an algorithm to correlate river flow depth with water surface reflectance using high resolution images. Smith & Pavelsky (2008) estimated river discharge, propagation speed and hydraulic geometry using MODIS data for Lena River in Siberia. Papa et al. (2010) conducted a study to derive monthly discharge on the Ganges and Brahmaputra River by using TOPEX-Poseidon, ERS-2 and ENVISAT satellite imagery. Hirpa et al. (2013) conducted a study to forecast the Ganges and the Brahmaputra River flow and water level by performing passive microwave remote sensing of 22 upstream location.

2.2 MICROWAVE APPROACH FOR FLOW ESTIMATION

Different study has been conducted so far relating river flow, water level estimation for flood forecasting using microwave satellite imagery.

2.2.1 Satellite Data

The microwave spectrum is usually defined as electromagnetic energy ranging from approximately 0.3 GHz to 300 GHz in frequency. After absorbing the Sun's shortwave radiation, longwave radiation is emitted from earth. Having a longer wavelength, microwave radiation is not disturbed by cloud interference and also data retrieval is possible even in night when solar illumination is absent. These attributes allow for frequent data retrievals on a global basis (e.g. pixel spatial resolutions of ~10km, daily or near-daily basis). Factors that affect microwave brightness are:

1. Sensor calibration properties
2. Perturbation of the signal by land surface changes
3. Contrast between land and water at the frequency being used. (Brakenridge et al., 2012)

Brightness Temperature is the temperature of a blackbody with the same temperature. As rivers rise and discharge increases, floodplain water surface area increases.

2.2.2 Methodology Development

Initially it was found out that orbital sensor has the capability to measure discharge along braided river (Smith, 1997). Technique was to observe water level change from space as water spread over the levee as water stage rises. Moreover satellite technology have an advantage of daily availability. Brakenridge, Nghiem, Anderson and Chien (2007) developed a daily monitoring of river systems based on AMSR-E data. The methodology uses the 36.5 GHz horizontal polarized band of the descending (nightly) orbit with a footprint size of approximately 8×12km. The aim of the method is to observe riverine inundation increment (land cover change) of a flood event. Due to the different thermal inertia and emission properties of land and water, the observed microwave radiation has low brightness temperature for water and high for land as water has more absorption capacity than land surface (De Groeve, et. al., 2007). In spite of the great radiation dissimilarity of water and land cover, the raw brightness temperature observations cannot be used to reliably detect changes in surface water area. This is because brightness temperature measures are influenced by other factors such as physical temperature, permittivity, surface roughness and atmospheric moisture (De Groeve, 2010). While the relative contribution of these factors cannot be measured, they are assumed to be constant over a larger area. Normalization of signal was done by comparing a wet signal received over a river channel with a dry signal without water cover noise factors. This normalization was implemented where the brightness temperature values of the measurement or wet signal were divided by the calibration or dry observations (referred to as M/C ratio). Results of this kind of calibration eliminates daily and seasonal temperature changes, soil moisture, vegetation influences by assuming that the wet and the dry location has the same properties except for the water surface extent (De Groeve et al., 2007).

2.2.3 Selection of Image Specification

Initial approach was to use Space-borne synthetic aperture radars (SARs) data. It was found that single polarization, C-band SARs are effective for mapping smooth, open water bodies though vegetation, trees, wind or flow turbulence making inundated areas problematic. L-band SARs can penetrate forest canopies and often display increased returns over flooded forest produced by a double bounce mechanism between inundated tree trunks and the water surface (Smith, 1997, Bjerklie,et.al., 2005). Limitations of this selection criteria lead to use of MODIS data (Brakenridge, et. al., 2005). But MODIS data is often disturbed by cloud interference. For that reason use of longer wave length microwave temperature brightness data was started to be used (Brakenridge, et.al., 2007; De Groeve, et. al., 2007). This technique used 36.5 GHz horizontal polarization band. It is observed that 36.5 GHz frequency is very sensitive for water surface (Sun & Lu, 2005) and horizontal polarization shows maximum temperature brightness value (**Figure 2.1**).

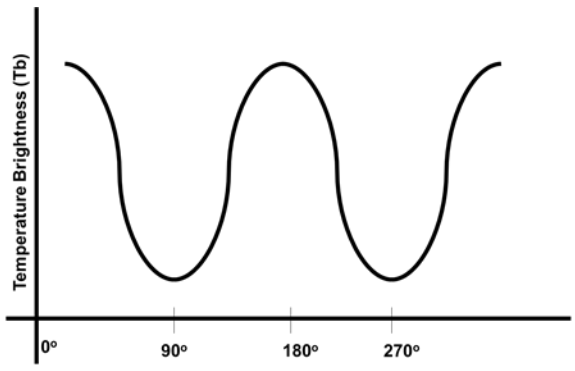

Figure 2.1: polarization effect on temperature brightness.

2.3 WATER REFLECTANCE APPROACH FOR FLOW ESTIMATION

Reflectance is the total amount of radiation incident on a specific surface. Different surface has different reflectance. Different band has different properties of reflectance as water interacts differently with different bands of spectrum.

2.3.1 Satellite Data

Surface reflectance has a wide band of spectrum from violet (380 – 450 nm), blue (450 – 495 nm), green (495 – 570 nm), yellow (570 – 590 nm), orange (590 – 620 nm), red (620 – 750 nm) near infra-red (750- 1400 nm) to short, medium and low infrared band. Landsat satellite has an instrument to acquire images from 0.43 μm to 12.51 μm (L8 OLI/TIMS). This data is available in 30 m resolution. Terra satellite also has an instrument to acquire images from 0.47 μm to 21.30 μm (MOD09), but its resolution is coarse. Durand, Rodriguez, Alsdorf, & Trigg (2010) used radar interferometer data of Surface Water and Ocean Topography (SWOT) mission to estimate river height, slope and width. Fakhruddin & Hassan (2003) used LANDSAT TM and RADARSAT SAR data to estimate flow for Brahmaputra River Bangladesh. Majozi (2011) used Medium Resolution Imaging Spectrometer (MERIS) data of ENVISAT satellite to estimate the euphotic depth of Lake Naivasha.

2.3.2 Theory behind Water Reflectance approach

Water has a unique property of reflectance. Water absorb higher wavelength of spectrum. Blue band of spectrum has a high reflectivity whereas red band is absorbed after few meters of depth of water. This unique property shows a relation between flow depth with reflectance difference of two nearby bands of spectrum i.e. blue band and green band. Based on this principle Gordon et al. (1983) developed an technique to estimate phytoplankton pigment concentration. Stumpf, Holderied, & Sinclair (2003) used similar algorithm to estimate water depth for variable bottom types. Water surface reflectance (R_w) is found by correcting the total reflectance (R_T) for the aerosol and surface reflectance, as estimated by the near-IR band, and for the Rayleigh reflectance R_r. According to Stumpf, Holderied, & Sinclair (2003) water surface reflectance, $\mathbf{R_w = R_T(\lambda_i) - Y(\lambda_i) R_{T(NIR)} - R_r(\lambda_i)}$, where, Y is the constant to correct for spectral variation. Gordon et al. (1983) estimates Y as angstrom exponent. Angstrom exponent is a measure of the spectral dependence of aerosol optical depth. MODIS atmospheric science team provides Angstrom exponent for the aerosols over Land based on 470 and 660 nm optical depths. Subscript i denotes a visible channel, and subscript NIR denotes the near-IR channel.

2.3.3 Selection of Image Specification

Gordon et al. (1983) developed the algorithm using color scanner images of NIMBUS-7. After that Stumpf et al. (2003) used high resolution IKONOS satellite imagery for depth estimation. LANDSAT provides similar surface reflectance imagery with 30 m resolution. Most of the river in Nepal is wide enough to fit LANDSAT single pixel. But LANDSAT images are available twice in a month and moreover in monsoon, images are overwhelmed with cloud cover.

2.4 HYDROLOGICAL MODEL

Hydrological modeling is a representation of simplified and conceptual circulation of water cycle. This model helps to understand the interaction among rainfall, sub-surface water and snow storage. MIKE 11 NAM is a lumped, conceptual rainfall-runoff model. This is based on physical structures and equations used together with semi-empirical ones. Lumped model assumes each catchment as a single unit. Average values of parameters and variables are used for the entire catchment. Final parameter estimation is performed by calibration against time series of hydrological observations (DHI, 2012).

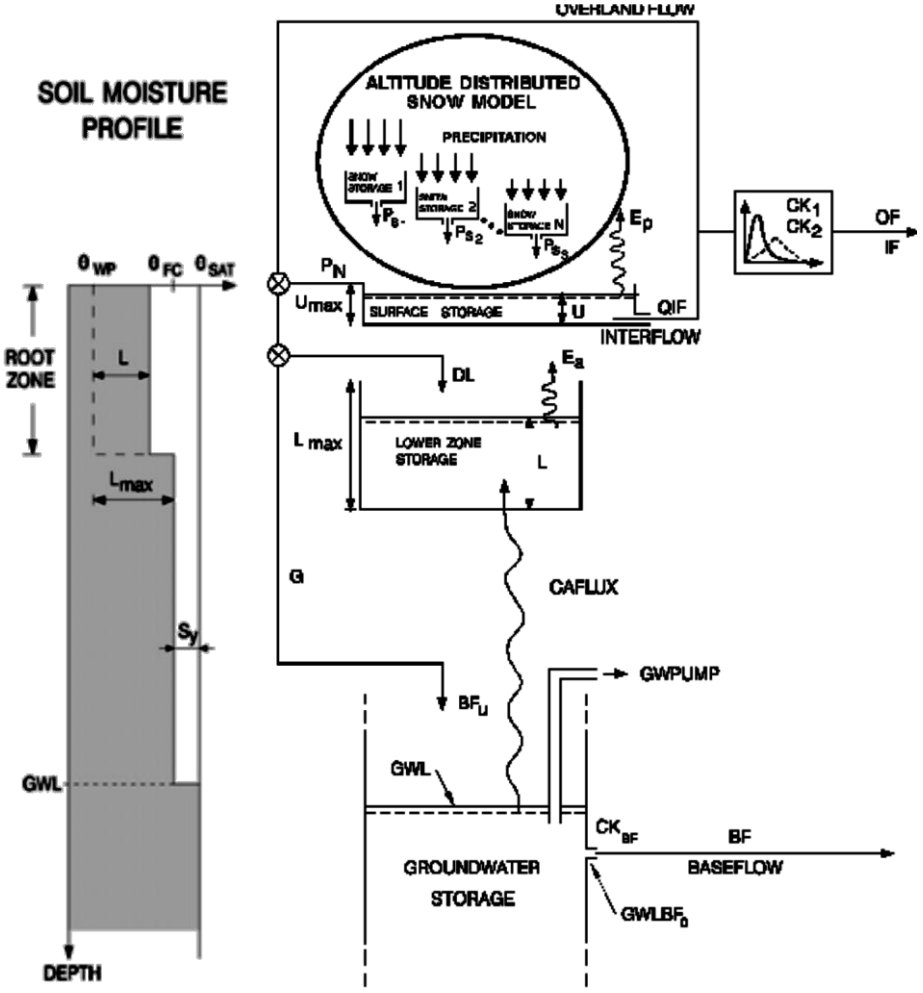

Figure 2.2: Structure of the NAM model with extended snow module

This hydrological model represents the rainfall-runoff process by continuously accounting for the water content in four different and mutually interrelated storages. These storages are (a) Snow storage, (b) Surface storage, (c) Lower or root zone storage and (d) Groundwater storage. It also allows man-made interventions i.e. irrigation and groundwater pumping.

Hydrologic model requires hydro-meteorological data i.e. rainfall, evaporation, temperature, discharge, water level etc. These data require quality checking, appropriate correction, validity, consistency before using as model input.

2.4.1 TRMM rainfall correction

Ines & Hansen (2006) used this simple technique to remove the biasness from GCM rainfall. This correction is also suitable for TRMM rainfall correction.

$$\text{Multiplicative Shift, } x_i' = x_i \times \frac{\text{mean Observed rainfall}}{\text{mean TRMM rainfall}}$$

2.4.2 Altitude effect over Hydrological model

In mountainous areas temperature, precipitation and snow cover vary significantly within a single catchment. The runoff simulation was improved by dividing the catchment into smaller zones and maintain individual snow storage calculations in each zone. The altitude-distributed snow model calculates water in altitude zones using the degree-day approach. During cold periods precipitation is retained in the snow storage from which it is melted in warmer periods. The shift between precipitation in the form of rain and snow usually takes place when the air temperature is 0°C (DHI, 2012).

2.5 HYDRODYNAMIC MODEL

Main principle behind hydrodynamics of river is mathematically expressed by the kinematic, diffusive and dynamic Saint Venant equations. MIKE 11 HD model uses the finite difference approach and double sweep algorithm to solve the unsteady state equations. It also has capability to model irregular open channel and varied flow resistance through different branches of network. It can simulates flow over hydraulic structures (DHI, 2012).

Continuity:

$$\frac{\partial Q}{\partial x} + \frac{\partial A}{\partial t} = q$$

Momentum:

$$\frac{\partial Q}{\partial t} + \frac{\partial\left(\frac{\alpha Q^2}{A}\right)}{\partial x} + gA\frac{\partial h}{\partial x} + \frac{gQ|Q|}{C^2AR} = 0$$

Where,

Q = discharge (m^3/s)

A = Flow area (m^2)

Q = Lateral inflow (m^2/s)

H = Stage above datum (m)

C = Chezy resistance coefficient ($m^{1/2}/s$)

R = Hydraulic radius (m)

A = Momentum distribution coefficient

2.6 FLOOD FORECASTING MODEL

Flood forecasting is an important step for flood management. Flash floods are defined to be flood events where the rising water occurs during or a matter of a few hours after the associated rainfall. Physically based models are common to forecast flood. It has an advantage to study flood control strategies and planning besides flood forecasting (Stronska, Kitowski & Jorgensen, 1999). Flood forecasting systems provide predictions of the inflow in the downstream reaches and warnings to local authorities and the affected population. Literature has shown that different methods used for modeling of river flow. Artificial neural networks (ANN) have been recently practiced more often as an efficient alternative tool for modeling of complex hydrologic system. Some of the studies are summarized below:

Table 2.1: SUmmary of different Flood forecasting model

Model	Correlation	RMSE	Author	River Basin
Adaptive Neuro-Fuzzy Interference System (ANFIS)	0.44 - 0.97	9.98 - 130.78 cms	Mukerji et al. (2009)	Ajay River Basin
Adaptive Neuro-Fuzzy Interference System (ANFIS)	0.894 - 0.935	6.322 - 33.972 cms	Firat (2008)	Seyhan River and Cine River
Adaptive Neuro-GA Integrated System (ANGIS)	0.52 - 0.98	8.16 - 119.28 cms	Mukerji et al. (2009).	Ajay River Basin
Artificial Neural Network (ANN)	0.33 - 0.96	16.9 - 146.31 cms	Mukerji et al. (2009)	Ajay River Basin
Artificial Neural Network (ANN)	0.91	16%	Wardah et al. (2008)	Klang River Basin
Artificial Neural Network (ANN)	0.902 - 0.921	0.68 - 0.90 m	Panda et al. (2010)	Mahanadi River Basin
Auto-Regressive (AR)	0.854 - 0.914	6.99 - 39.344 cms	Firat (2008)	Seyhan River and Cine River
Back-Propagation Neural Network (BPNN)	> 0.9	0.021 - 0.051	Chang et al. (2010)	Shigo drainage canal
Bootstrap Based Artificial Neural Networks (BANNs)	Significant Correlation	0.02 - 0.13 m	Tiwari & Chatterjee (2010)	Mahanadi River Basin
Ensemble Square-Root-Filter (EnSRF)	0.027 - 0.82	164.1% - 201.9%	Chen et al. (2013)	Cobb Creek and Chuzhou watershed
Feed Forward Neural Networks (FFNN)	0.826 - 0.899	7.551 - 43.595 cms	Firat (2008)	Seyhan River and Cine River
Generalized Regression Neural Networks (GRNN)	0.865 - 0.928	6.864 - 37.189 cms	Firat (2008)	Seyhan River and Cine River
Linear Regression	0.823 - 0.935	2,546 - 3,271 cms	Birkinshaw et al. (2010)	Mekong River Basin
Hydrodynamic Model in MIKE11	0.912 - 0.921	0.99 - 1.00 m	Panda et al. (2010)	Mahanadi River Basin
Physics Based Distributed (PBD) Hydrologic Model	0.73 - 0.98	1.77 m	Looper & Vieux (2012)	Austin, Texas
Power Law Regression	0.77	16%	Wardah et al. (2008)	Klang River Basin

*correlation indicates the amount of error between simulated result with observed data

CHAPTER 3
STUDY AREA AND DATA COLLECTION

3.1 THE KOSHI RIVER BASIN

Study area of this research is the Koshi River Basin. Koshi Basin (**Figure 3.1**) has area of 87,480 km^2 (India 19,685 km^2, Nepal 39,407 km^2 and China 28,368 km^2) (**Table 3.1**). According to Bharati, Gurung, & Jayakody (2012), the basin can be divided into the trans-mountain, central mountain, eastern mountain, eastern hill and central hill regions. It is observed that precipitation is highest in the central mountain and eastern mountain regions during both the dry and wet seasons.

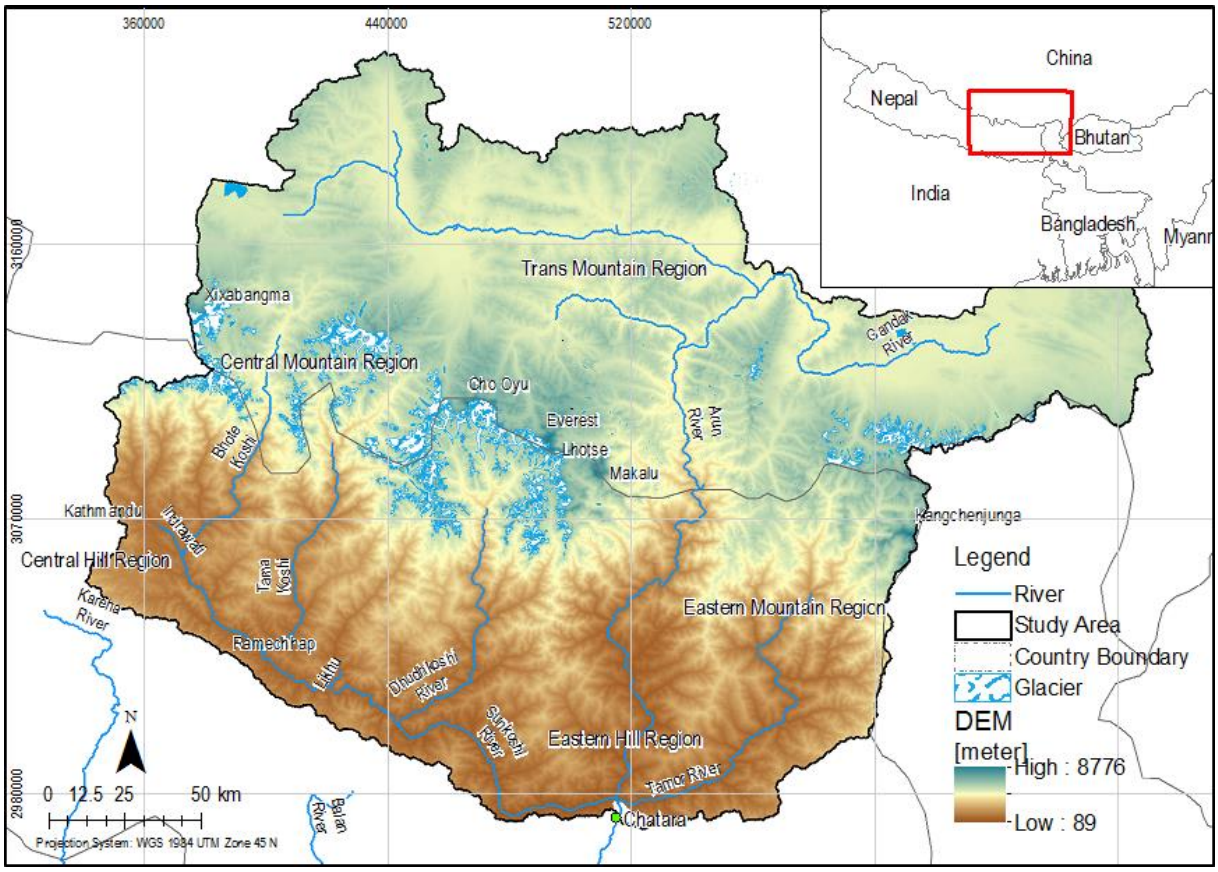

Figure 3.1: The Koshi River and Regions with elevation profile

Evapotranspiration is highest in the central and eastern mountain regions followed by the mid-hills. This watershed drains water into Saptakoshi River through Chatara. In the downstream, Koshi river meets with the Ganges River.

3.1.1 The Koshi River System

The Koshi river system is the largest river system in Nepal. It originated from Tibet and continues through the Himalayas and terai region before reaching the Ganges River in India at Kursela. Mount Everest (8,848 m) is the highest mountain peak in the world and the Koshi River drains water from this mountain system. The average elevation of the Koshi river basin is 3,800 m. This river system has an elevation range from below 100 m the Ganges plains to more than 8,000 m in the great Himalayan alpine mountain system. Koshi or Saptakoshi

River has a number of tributary i.e. Tamor Koshi, Arun Koshi, Sun Koshi, Indrawati, Dudh Koshi, Tama Koshi and Likhu Khola, Indrawati River. Among these rivers, Tamor Koshi originating from Mt. Kanchenjunga in the east, Arun Koshi from Mt. Everest in Tibet and Sun Koshi from Mt. Gosainthan farther west. These tributaries flows through and side of Mount Everest. Sun Koshi, Tamor and Arun meet at Tribeni from west, east and north respectively and from there the river flows through a narrow gorge passing the gauging station at Chatara. After this confluence, the river is called 'Sapta Koshi' or Koshi (which means Seven Rivers).

Table 3.1: Tributaries of the Koshi River

Name	Area (km^2)	Location
Arun	27,631.23	Tibet, Nepal
Bhote Koshi	3,612.62	Tibet, Nepal
Indrawati	1,228.98	Nepal
Tama Koshi	5,345.34	Tibet, Nepal
Dudh Koshi	4,066.94	Nepal
Likhu Khola	1,051.35	Nepal
Sun Koshi	2,840.99	Nepal
Tamor	6,117.53	Nepal

Before reaching the Ganges River, the flow of the Koshi is controlled by Koshi barrage or Bhimnagar barrage which is located in Nepal-India border (Nepal, 2012). The Koshi River has a very high sediment transport capacity. After reaching Chatara, river flow velocity becomes slow and sediment start settling. This sediment deposition trigger course shift. The Koshi River migrated westward throughout last 250 year. The three-dimensional geometry of the Koshi megafan is similar to those of typical alluvial fans, but with much gentler gradient (0.05^o–0.01^o) and with larger area (>10,000 km^2). (Chakraborty et. al., 2010). The Koshi River has an average water flow of 2,166 m^3/s and it contributes 340 MCM water to the Ganges River (Jain, Agarwal, & Singh, 2007).

3.1.2 Climate and Hydrology

The climate is generally influenced by the Indian monsoon system. The summer monsoon dominates the climate from May to September and westerly circulation dominates from November to March which is known as winter monsoon. Within Nepal, the onset of summer monsoon starts from the eastern part from mid-June to September (Ueno, Toyotsu, Bertolani, & Tartari, 2008). There are primarily four seasons in the region. They are: the winter (December - February), the pre-monsoon period (March-May), the monsoon period (June-September) and the post-monsoon period (October-November) (Shrestha, Wake, Mayewski, & Dibb, 1999).

The basin has tropical to sub-tropical climate at the lower altitude (Terai and Siwalik) characterized by a hot and wet summers and mild and dry winters. The Middle Mountain (the Lesser Himalaya) exhibits a warm temperate monsoon climate. The higher altitude area has sub-alpine to alpine climate up to 4,800 m associated with low temperatures. Higher than snowline exhibit very cold climatic conditions where the temperature remains below zero degree Celsius throughout the year which provides conditions for the development of

glaciers in the region (Mool et.al, 2002). About 80% of the total annual precipitation occurs during the months of June through September, however, this varies annually (Ueno et al., 2008). It is observed that nearly 73% rainfall occurs from June to September near Chatara.

3.1.3 Topography

Koshi River basin topography is a result of the emergence from the tectonic uplift of sedimentary deposits (Dahal & Hasegawa, 2008). Topography of this basin can be divided into the following zones: Terai, Siwalik (Sub-Himalaya), Lesser Himalaya (Middle mountains), Higher Himalaya and Trans Himalaya (Shrestha et al., 1999; Upreti, 1999). **Figure 3.2** shows the topographic division of Koshi river basin. These zones contain some unique properties i.e. elevation variation, slope, relief characteristics. This properties has a great influence on local climate.

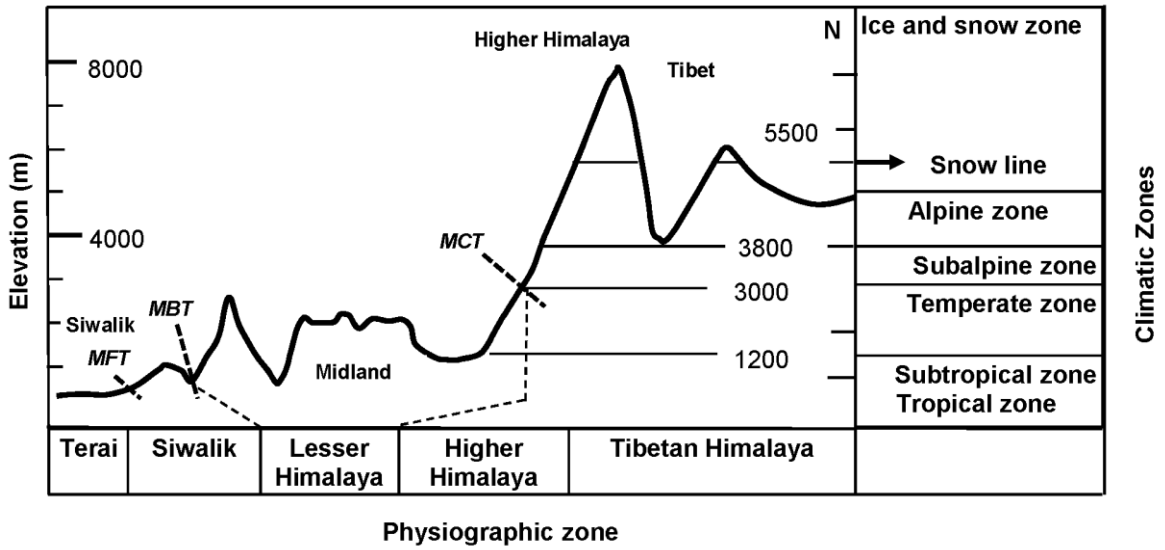

Figure 3.2: Generalized cross section of the Koshi basin region (Nepal, 2012)

Elevation range of terai region is 60-330 m and it is located along the southern part of the basin. This is a narrow strip of flat alluvial terrain (Nepal, 2012). Siwalik zone is located after terai region and elevation varies from 200 to 1,500 m. The region contains dry and unconsolidated soil materials (Upreti, 1999). To the north of the Siwalik range, the Lesser Himalaya is located. Elevation has a range from 500 m to 3,000 m. The Higher Himalaya region is located to the north of the Lesser Himalaya and is characterized by an abrupt rise of topography forming steep Himalayan peaks (Nepal, 2012). Mt. Everest (8848 m) is located in higher Himalayan region. This region has several more peaks exceeding 8,000 m height.

3.1.4 Glaciers and glacial lakes

There are about 779 glaciers in the Koshi river basin which covers an area of about 1,410 km^2 with an estimated ice reserve of 152 km^3. There are 1,062 lakes in this basin covering 25 km^2. These lakes and glaciers have a highly erosive nature. In the recent studies it is observed that glaciers and glacier lakes are exhibiting a retreating nature and its rate is higher than the formation of glacial lakes (Mool et al., 2002). About 12% glacier area is retreated from 1976

to 2000 in Dudh Koshi river basin. In the recent decade, Himalayan glaciers have been shrinking and retreating at a faster rate (Bajracharya & Mool, 2009).

3.1.5 Flood and Inundation

The Koshi River is a flood prone river. Rapid and frequent avulsions of its course is a common phenomenon for this river. After flowing through the Himalayas, it enters India near Bhimnagar. It flows through the plains of north Bihar and joins the Ganga River near Kursela, after traversing for 320 km from Chatara. This river has a history of westward movement through its path (Bapalu & Sinha, 2005).

A dike was breached in 18 August 2008 near Kusaha around 12 km upstream from the barrage and the river 120 km shifted eastward. This avulsion was triggered by a breached in the eastern embankment and 80 – 85% flow of the river was diverted into the new course. After nine month, the river was diverted back into the pre-2008 channel. The resulting flood left nearly 527 lives inundated, 116 thousands Hacter of land and left 234 thousand people homeless. Devkota et.al. (2012) showed that 2008 event was occurred at normal hydrological year. This incident was rather triggered by the dike breach. Koshi exhibits a highly variable discharge.

Meena (2012) developed a models to estimate flood inundated areas for the Koshi River Basin. Parameters i.e. rainfall, discharge, water level, soil moisture, TRMM rainfall and other variables were used as input to develop models for flood inundation mapping. Analysis was done for year 2006, 2007 and 2009. This study reveals flood inundation map (**Figure 3.3**) of the Koshi River basin.

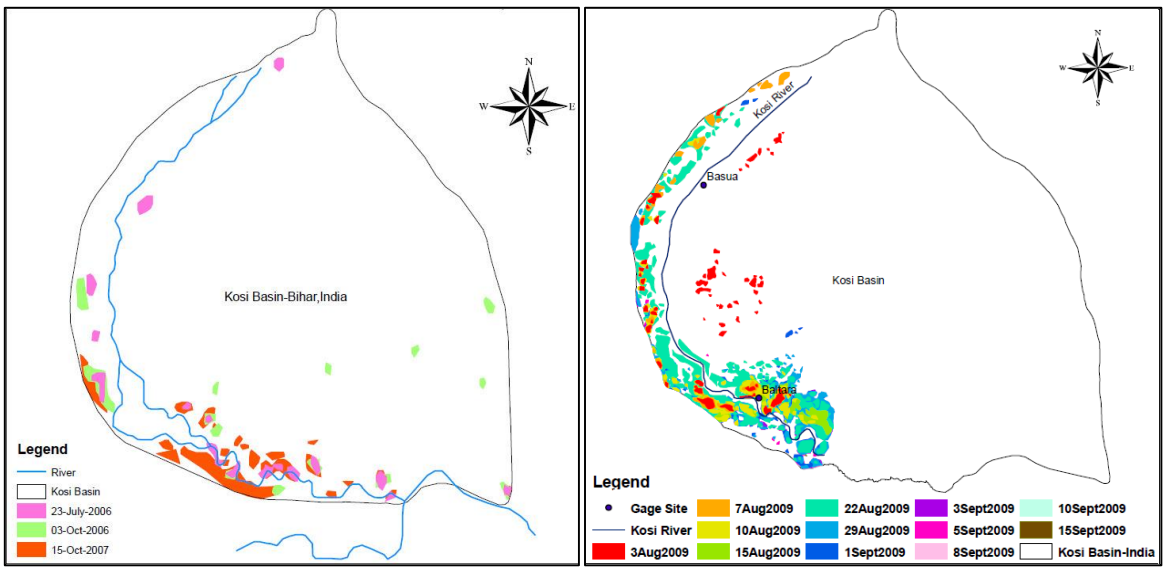

Figure 3.3: Flood inundation map for Koshi river basin (Meena, 2012)

Flood in Rajbiraj, Biratnagar, Purnia, Bihar is basically caused by the Koshi River. In the years 1978, 1987, 1998, 2003, 2004, 2007 and 2008 Bihar witnessed high magnitudes of flood. In year 2003 maximum discharge of about 1,100 m^3/s water passed through Koshi River and in year 2004 flood maximum discharge was about 8,100 m^3/s. A detailed picture of historical flood damage is drawn below:

Table 3.2: Historical Flood Damage Estimation caused by the Koshi River

Year	Affected People (million)	Damaged Property (million USD*)	Death
1998	-**	74	-
1998	-	48	-
2000	9	13.5	336
2001	9.1	73	231
2003	7.6	12	251
2004	21.2	251	885
2008	4.9	21	258
2010	0.7	0.8	32
2013	5.9	-	150

Source: Flood Management Information System (FIMA) Bihar

* Actual damage property was in Indian Rupees. Conversion rate of 19/09/2013 was used

** Blank data indicates unavailability of data

3.2 DATA COLLECTION

Different hydro-meteorological and topographic data is required to develop, calibrate, and validate the hydrologic, hydrodynamic and flood forecasting model. DHM, ICIMOD, IWM are main source of hydro-meteorological and topographic data. ASTER 30 m DEM, LANDSAT, MODIS, Temperature brightness data will be acquired from NASA and JAXA websites.

3.2.1 Topographic Data

ASTER G-DEM data of October 2011 was collected to analyze the local topography. After collection, all the pixel was mosaicked. This data was used for longitudinal profile extraction and area- elevation evaluation. Also LANDSAT data (L-8) was collected for year 2013 as well as L-7 data for previous years. This data was used to develop remote flow estimation technique.

3.2.2 Hydro-meteorological Data

Daily rainfall data was collected from TRMM Online Visualization and Analysis System (TOVAS) where average rainfall was available in 25 km×25km pixel. To perform bias correction, daily rainfall data was collected from Aphrodite (http://www.chikyu.ac.jp/precip/index.html). Also observed rainfall data of DHM stations namely Okhaldhunga, Bhanjyang, Salleri, Diktel, Chainpur, Leguwa ghat, Terhathum, Chatara, Tumlingtar, Dingla, Lungthung, Taplejung, Memeng Jagat, Phidim, Dovan, Nagdaha, Charikot, Jiri, Manthali, Chaurikhark and Pakarnas. Temperature data was collected from Aphrodite. Evapotranspiration data was collected from DHM.

3.2.3 Maps and Imageries

Brightness temperature (T_b) image of 36.5 GHz H-polarization is best sensitive with water. This data is acquired with a microwave sensor mounted on satellite. Microwave sensor is mounted on few satellites i.e. AQUA, TRMM, and SHIZUKU. Apart from AQUA satellite, other latest microwave data is freely available for research. As AQUA satellite is decommissioned, AMSR-E data is not available lately. It is only available from 2002-2011. But as this study is modelling past data, AMSR-E data can also be used. AMSR-E data is

collected from JAXA website (http://gcom-w1.jaxa.jp). This website provides daily worldwide AMSR-E map upto November 2011. This is a level-3 (converted data from level 2 product, including previously defined global grid etc.) data with 25 km resolution. Image was collected from 2001 to 2008.

To develop water surface reflectance approach for remote flow estimation, LANDSAT (L-8 OLI/TIMR) imagery was downloaded from Earth Explorer (http://earthexplorer.usgs.gov) website. This website provides wide variety of satellite imagery. Land surface temperature (MOD11A1) data was also downloaded from this website.

3.2.4 Rainfall Forecast

Rainfall forecast data is available in different sources in global scale. National Center for Environmental Prediction (NCEP) provides Global Forecast System (GFS) model output for different climatic parameters including rainfall (http://www.nco.ncep.noaa.gov/pmb/products/gfs). This model predicts 16 days forecast. Data is available in 3 hours interval upto 8 days of forecasting. European Centre for Medium Range Weather Forecasts (ECMWF) also provides rainfall forecast data (http://data-portal.ecmwf.int).

CHAPTER 4
METHODOLOGY

4.1 METHODOLOGY FRAMEWORK

Figure 4.1 shows all the activities followed, stating from data collection to analysis of extreme events.

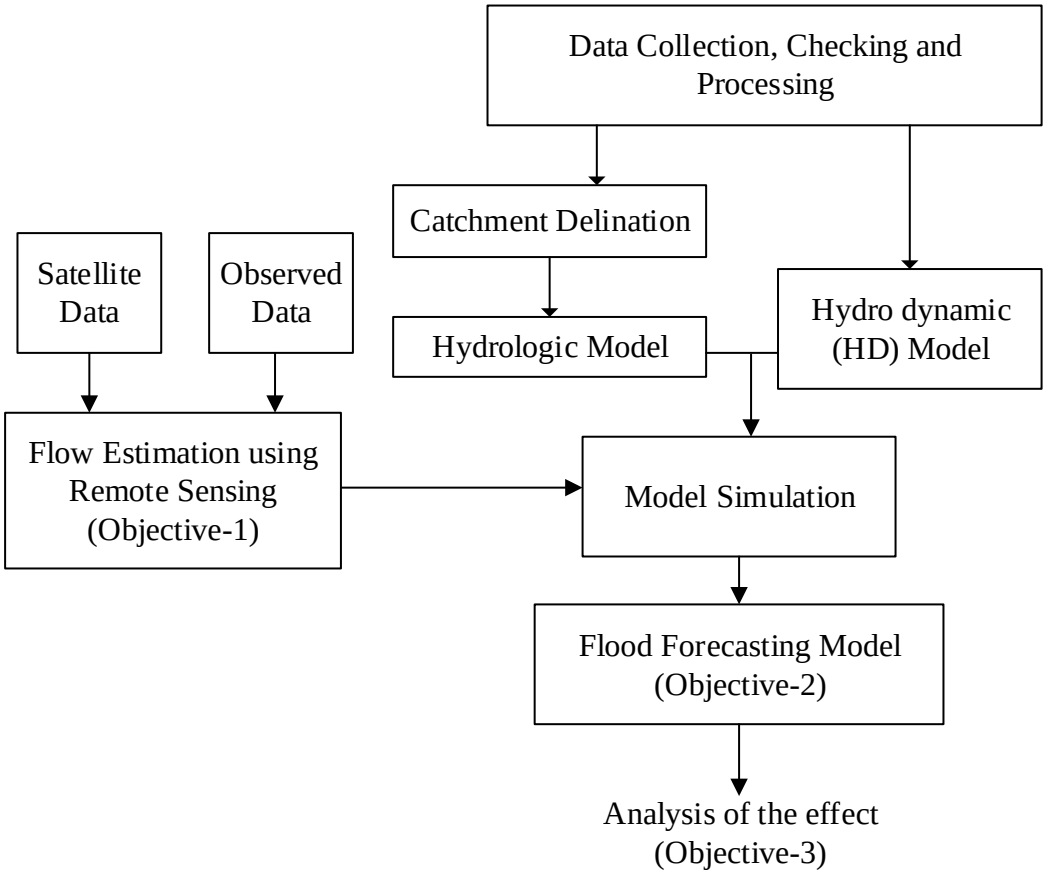

Figure 4.1: Schematic of research methodology

4.2 FLOW ESTIMATION USING PASSIVE MICROWAVE

Estimation of discharge from satellite imagery has its merits and demerits. It has a benefit of long term, regular availability of data, and avoidance of missing data, quality control and low cost. On the other hand, its accuracy is not always accurate, a certain range of error is expected every time, 50-60 year old data is not available as satellite technology was not developed then and vastly dependent on image processing.

Flood signal generation is based on temperature brightness imagery from satellite. Temperature brightness is the temperature a black body in thermal equilibrium with its surroundings would have to be to duplicate the observed intensity of a grey body object. For a black body, Planck's law gives that brightness is the amount of energy emitted per unit surface per unit time per unit solid angle and in a frequency range.

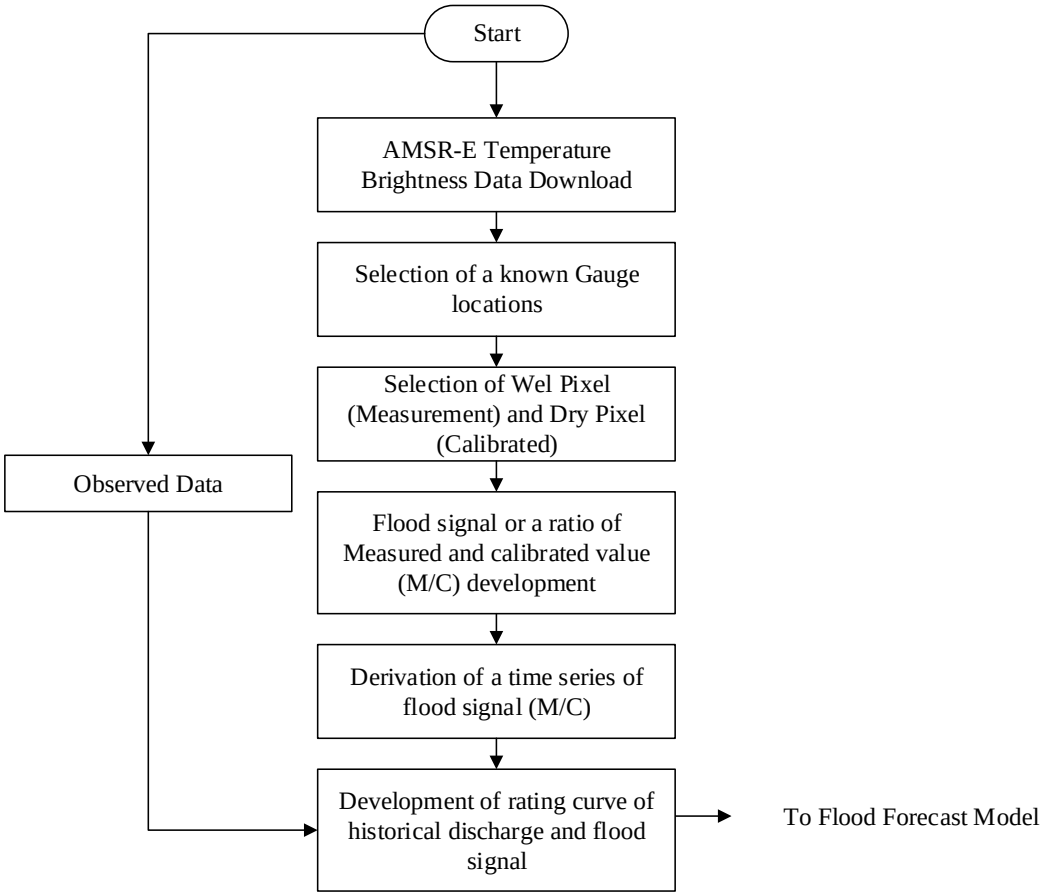

Figure 4.2: Flowchart for remote flow estimation using passive microwave

Due to the different thermal inertia and emission properties of land and water, the observed microwave radiation brightness temperature values is low for water ($T_{b,water}$) and higher for land ($T_{b,land} > T_{b,water}$). The raw brightness temperature observations are too noisy to detect changes in surface water area. This is because brightness temperature measures are influenced by other factors such as physical temperature, permittivity, surface roughness and atmospheric moisture. While the relative contribution of these factors cannot be measured, they are assumed to be constant over a larger adjacent area.

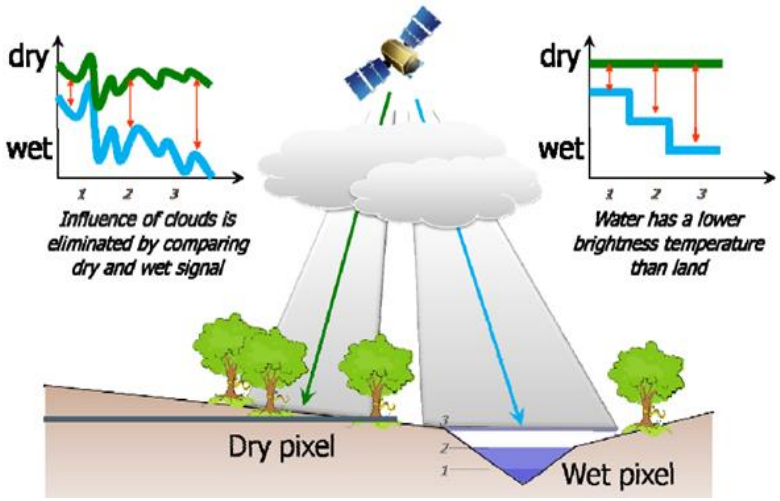

Figure 4.3: Principle for the flood signal

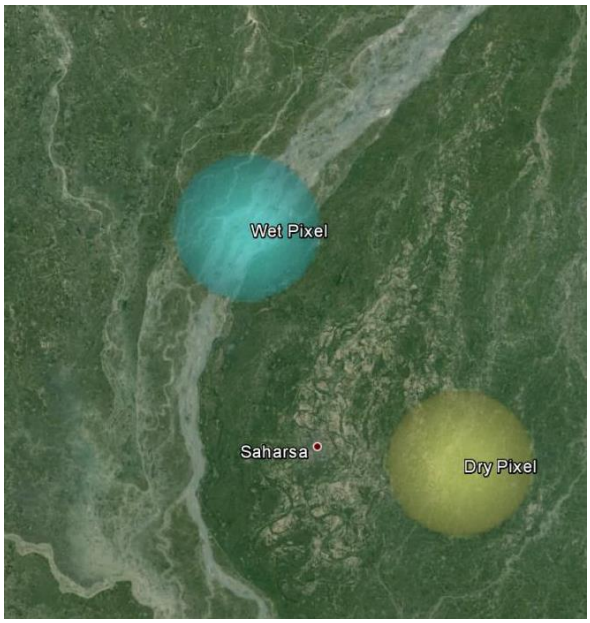

Figure 4.4: Observation sites over the Koshi River. Blue dot refers to wet pixel, green dot to dry pixel

Therefore, by comparing a "wet signal" received over a river channel of a potential inundation location with a dry signal without water cover the mentioned noise factors can be minimized. Thus normalization of the wet signal by the dry signal was implemented where the brightness temperature values of the measurement or wet signal (Tb_m) were divided by the calibration or dry signal (Tb_c), referred to as M/C ratio:

$$\frac{M}{C} = \frac{Tb_m}{Tb_c}$$

In order to distinguish between areas with permanent water (e.g. lakes or wide rivers) and areas with flood waters, change in flood signal should be observed. A grid based method should be used by utilizing daily brightness temperature grid and a way to obtain calibration values (M/C signal time series). The calibration brightness temperature for each pixel is calculated by selecting the maximum temperature brightness pixel from a grid of 7×7 pixels around the measuring wet observation pixel.

4.2.1 Rating Curve Development

A custom model was tool was developed using ArcGIS 10.1 is shown in **Appendix-A**. Process could be described as follows-

1. Selection of grid in a point shape file to extract raster pixel over study area.
2. Extraction of raster pixels.
3. Pixel over the study location was identified. This pixel was known as 'mCell'.
4. Calibration pixel [where Tb value is maximum in the grid] was identified. This pixel was known as 'cCell'.
5. After selecting both pixel, T_b value was determined from raster cell value using following formula, T_b = [Raster Value]/100 + 100.
6. After determining actual T_b value, mCell/cCell was done. This ratio is the corresponding flood signal.
7. Entire process was done in an iteration command.

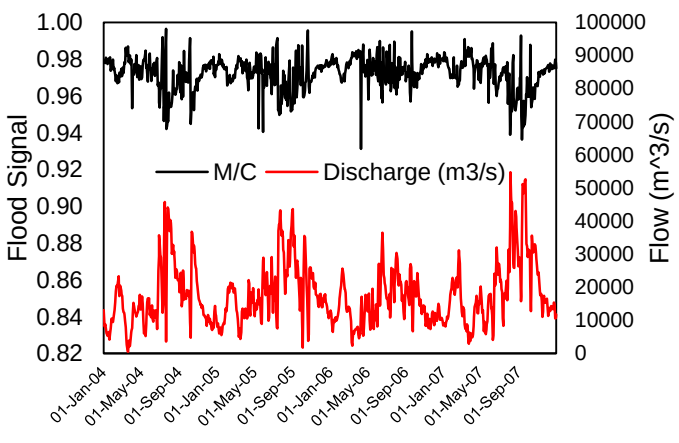

Figure 4.5: Correlation of M/C and Observed Discharge

Since lower M/C signals generally indicates increased water coverage and extreme events, negative anomalies in the time series of M/C for a given site is the indication of

flood. The value of anomalies can be related with flood events as well as discharge. Using historical temperature brightness image will lead to a rating curve. This rating curve will be relate flood M/C signal with actual river runoff and by using the rating curve equation, flow on the river is estimated. Following Figure illustrate a sample rating curve and a correlation with actual data.

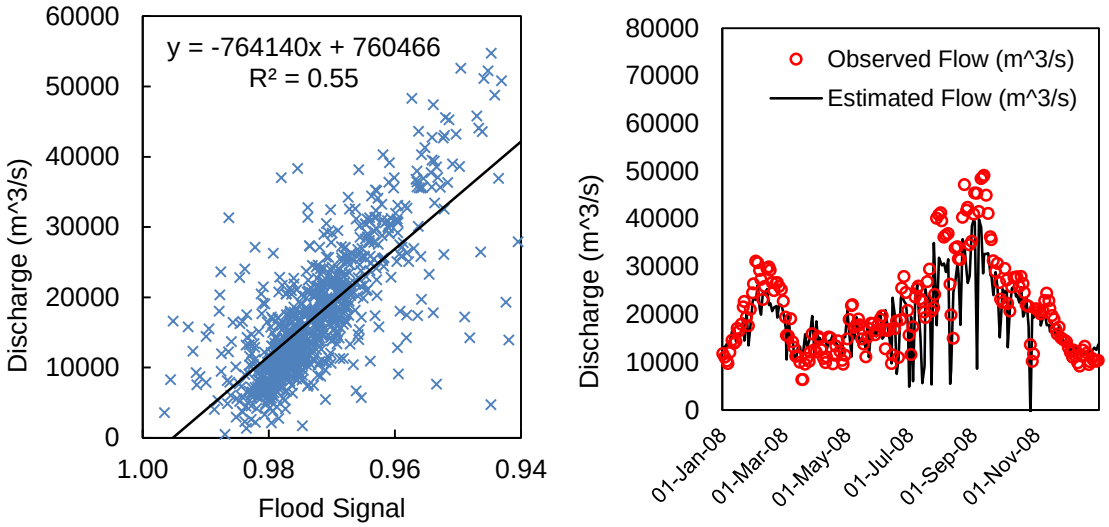

Figure 4.6: A sample Rating Curve and flow comparison near Akardh, India

4.2.2 Influence of Resolution:

Measuring pixel needs to contain river width with flood plain. This methodology is developed on the basis of flood water rise in the flood plain. It is assumed that water will have more spatial coverage with the increase of flow. In this case, if the pixel is entirely wet or submerged then that cell will exhibit the lowest temperature brightness (T_b) value. T_b value will remain same irrespective of flow increment.

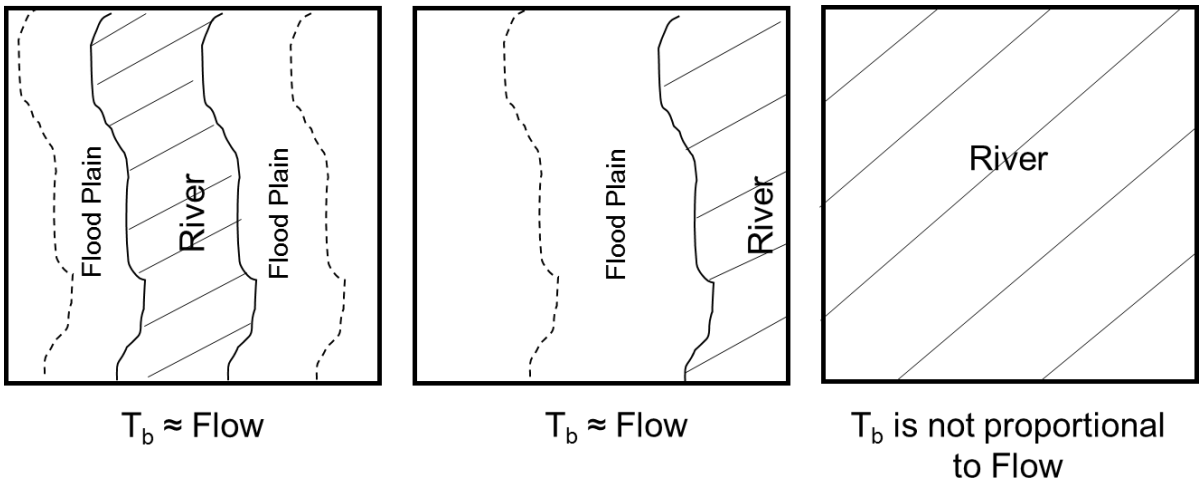

Figure 4.7: Effect of T_b value over spatial coverage within a pixel

4.2.3 Limitations

- In agricultural areas, irrigation of the measurement pixel can affect the signal as irrigated filed could reduce the temperature brightness value of the corresponding pixel.

- There are numbers of error involved in this technique. Satellite image processing contains error and flow estimation from rating curve also have some error. This two error affects the flow estimation.

4.3 SURFACE REFLECTANCE APPROACH FOR FLOW ESTIMATION

Flow estimation using passive microwave is not suitable for mountainous river. Mountainous rivers have some unique characteristics i.e. high velocity, narrow channel width, steep slope, no significant flood plain etc. As flow estimation technique using passive microwave imagery is based on spatial coverage of moisture, that technique is not suitable for the Koshi River (upstream of Chatara station).

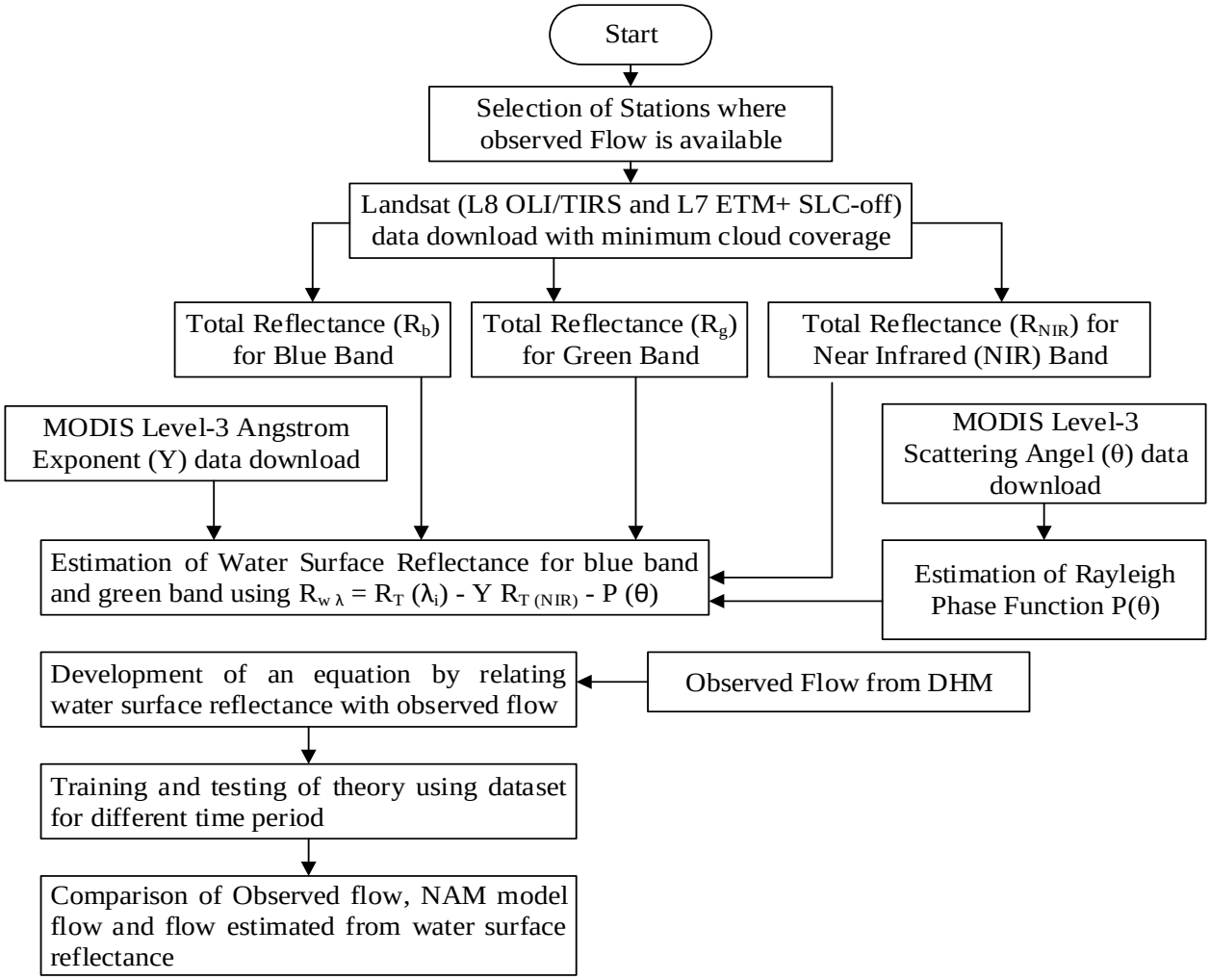

Figure 4.8: Flowchart for remote flow estimation using active microwave altimeter

The standard Landsat 8 products provided by the USGS EROS Center consist of quantized and calibrated scaled Digital Numbers (DN) representing multispectral image data acquired by both the Operational Land Imager (OLI) and Thermal Infrared Sensor (TIRS). The products are delivered in 16-bit unsigned integer format and can be rescaled to the Top of Atmosphere (TOA) reflectance and/or radiance using radiometric rescaling coefficients provided in the product metadata file (MTL file). OLI and TIRS band data can be converted to TOA spectral radiance using the radiance rescaling factors.

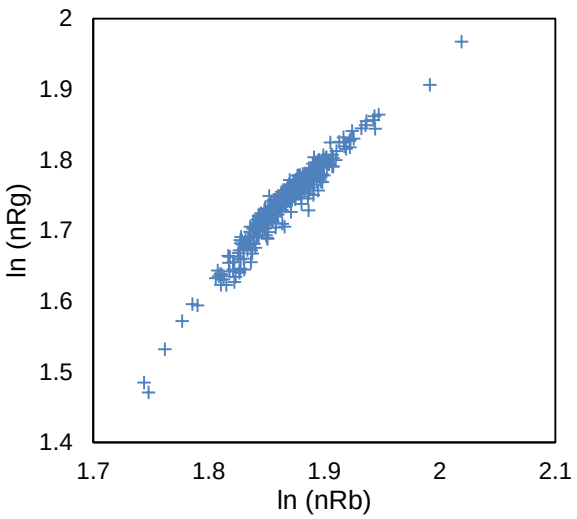

Figure 4.9: log transformation for Saptakoshi River (hilly portion of the river)

$L_\lambda = M_L \times DN + A_L$

Where,

L_λ= TOA spectral radiance (Watts/(m2 * srad * μm))

M_L = Band-specific multiplicative rescaling factor

A_L = Band-specific additive rescaling factor

DN = Quantized and calibrated standard product pixel values

Low wavelength of blue band has a high reflectance comparing high wave length of green band due to attenuation attribute of water.

Total reflectance, $R_T = \frac{\pi * L_\lambda * ds^2}{ESUN_\lambda * Cos\theta}$

L_λ = Spectral radiance

ds = Earth-Sun distance in astronomical units

$ESUN_\lambda$ = Mean solar exo-atmospheric irradiances

θ = Solar zenith angle in degrees = 90° - sun elevation

Stumpf et al. (2003) provided a formula of water surface reflectance as-

$R_w = R_{T(\lambda i)} - Y_{(\lambda i)} R_{T(NIR)} - R_{r(\lambda i)}$, were Rayleigh reflectance R_r proportional to phase function P(θ). The phase function P(θ) is described as the distribution of scattered radiation for one or set of particles. Rayleigh Reflectance is crudely approximated as a Phase function or P(θ) where

$P(\theta) = 0.75 \times (1 + \cos^2\theta) (\frac{1-\delta_R}{1+2\delta_R})$, here θ = aerosol scattering angel, δ_R = atmospheric Rayleigh reflectance. Vermote & Vermeulen (1999) gives an approximate value of δ_R as 0.0279. This gives phase function as $P(\theta) = 0.690543 (1 + \cos^2\theta)$. Aerosol scattering angel is the angle between the initial and final paths traveled by a scattered particle or photon. A techniques for flow estimation could be developed by using Stumpf et al. (2003) algorithm which are-

$$Q = m_1 \frac{\ln(nR_{w\,blue})}{\ln(nR_{w\,green})} - m_o$$

where Q = discharge (m^3/s), $R_{w\,blue}$ = water surface reflectance of blue band, $R_{w\,green}$ = water surface reflectance of green band, m_1, m_o = regression coefficient and n is a tunable coefficient to make sure that determinant is positive.

Here, $\mathbf{R_{w\lambda} = R_T(\lambda_i) - Y R_{T(NIR)} - P(\theta)}$

To use this technique, LANDSAT [L-8 OLI/TIRS (2013 – 2014), L-7 ETM+ SLC off (2001-2007)] cloud free level-1 data was downloaded. Angstrom exponent and scattering angel data was downloaded from MODIS Gridded Atmospheric Product (MOD08 Level-3).

4.4 HYDROLOGIC MODEL DEVELOPMENT

A lumped conceptual hydrologic model of Koshi basin will be used here. There are eight major sub-basin here namely Arun, Tamor, Sun Koshi, Dudhkoshi, Likhu, Tama Koshi, Bhote Koshi and Indrawati sub-basin. The MIKE 11 NAM model is a deterministic, lumped, conceptual model with moderate input data requirements. It simulates the rainfall-runoff processes occurring at the catchment scale. NAM forms part of the rainfall-runoff (RR) module of the MIKE 11 River modelling system. There are 58 rainfall station in the study sub-basins. Maximum available years of rainfall data should be acquired for this model development. There are mountain peaks sustain in the catchment. So temperature data will play a vital role. In this basin both arctic condition and tropical condition prevails, which requires wide variety of information. Parameter value should be influenced by previous research in this region.

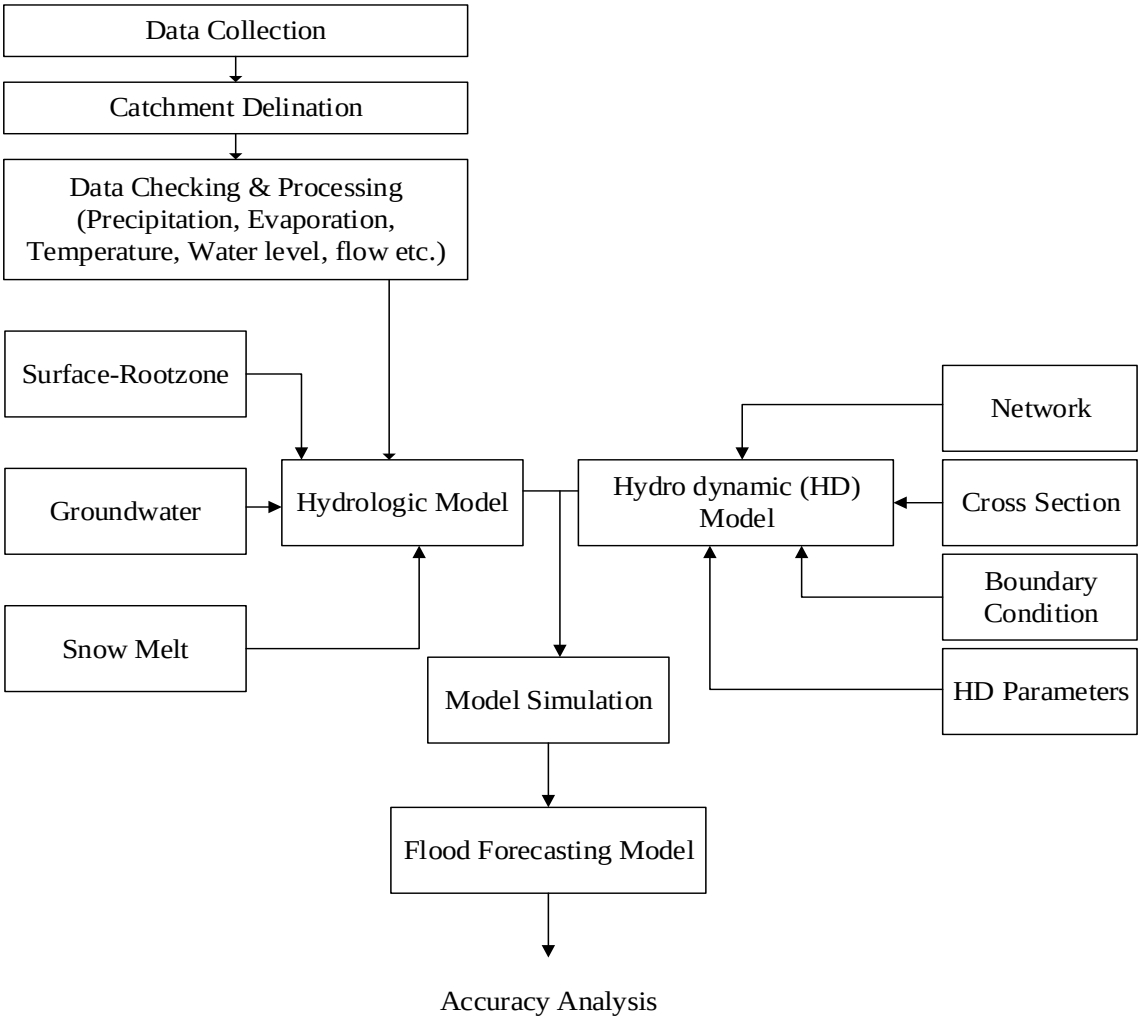

Figure 4.10: Specific Methodology Flowchart (relating Flood Forecasting)

4.4.1 Delineation of Sub-Catchment

Catchment delineation is done to create a boundary that represents the contributing area for a particular control point or outlet. Koshi River Catchment delineation was performed using

ASTER land elevation data. Total 49 catchment was delineated for entire Koshi River Basin. Chatara Station was taken as outlet. 10 Catchments (**Figure 4.7**) was lumped according to observed flow station availability (namely- Indrawati catchment, Bhote Koshi catchment, Tama Koshi catchment, Likhu catchment, Dudh Koshi catchment, Sun Koshi catchment, Arun1 & 2 Catchment and Tamor1 & 2 Catchment) in the upstream of Chatara Station.

4.4.2 Preparation of Data for Model

Hydrologic model needs mean catchment rainfall, evapotranspiration and area elevation of catchments particularly if the area is undulated i.e. hilly area in particular. There are 76 pixels of TRMM rainfall stations with 25km × 25km in and around the Koshi river basin area. Mean area rainfall (MAR) of each sub-catchment has been computed using weightage of the available rainfall stations. The weightage factors of rainfall stations for each sub-catchment have been computed by Thiessen Polygon Analysis using ArcGIS 10.1.

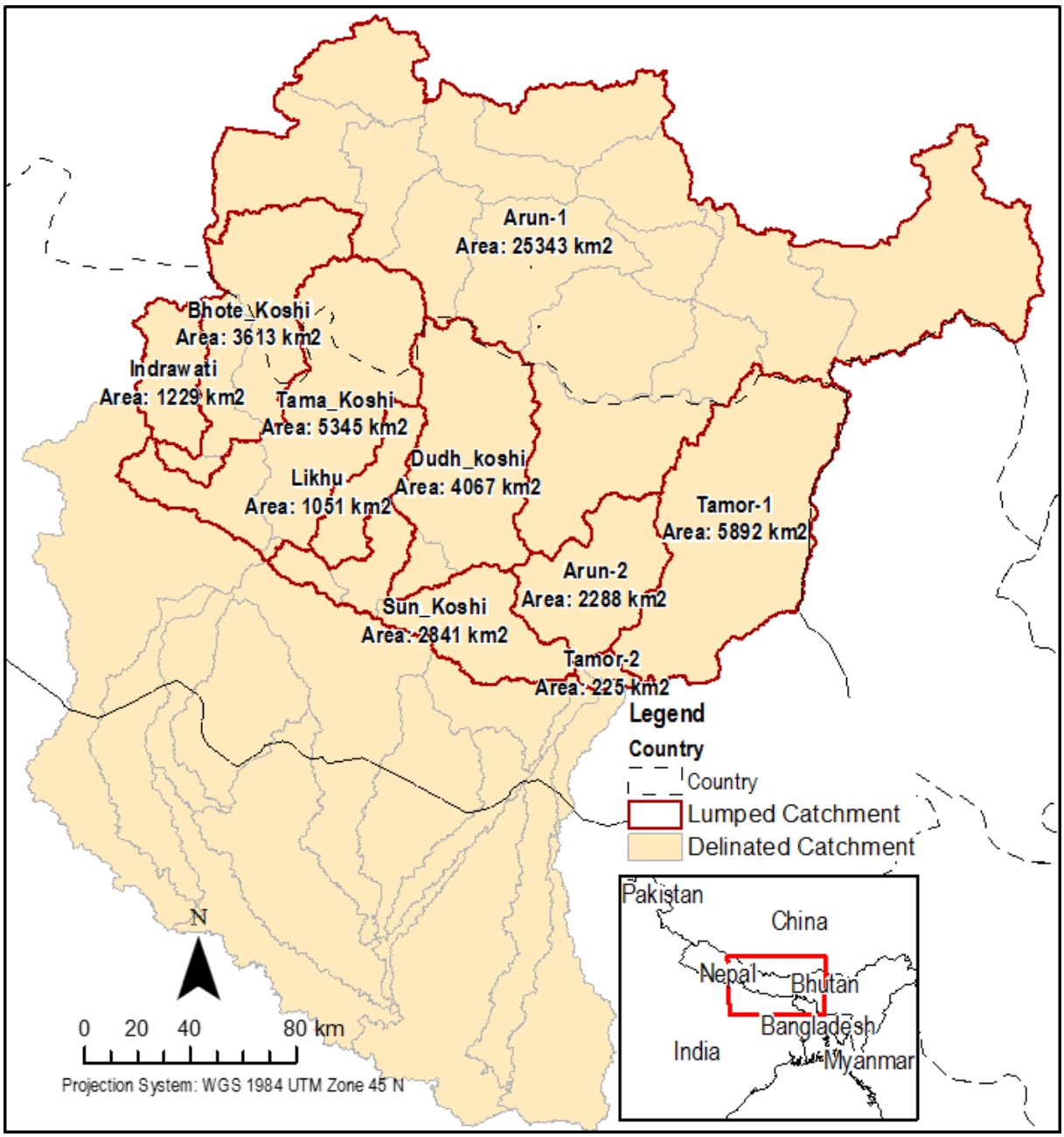

Figure 4.11: Catchment delineation

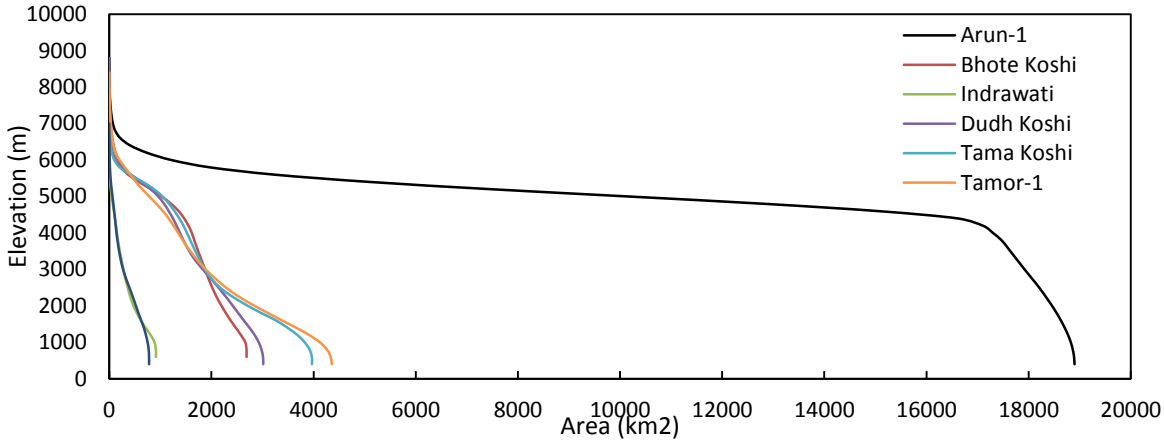

Figure 4.12: Hypsometric plot of the catchment

Temperature data was downloaded from Aphrodite website in same 76 stations like rainfall station. This data is has a resolution of 25°×25° and data is available upto 2007. After cross checking with NASA derived temperature this data was used in the model. An average temperature was derived for individual catchment. Evaporation and temperature data of 41 stations of entire GBM basin was available from ICIMOD. For the study area 3 elevation zones were considered namely below alpine zone (<4000 m), alpine zone (4000 m – 5000 m) and snow line zone (>5000 m) for data preparation.

4.4.2.1 TRMM Rainfall Data Correction

TRMM data does not always match with observed data. To use TRMM data as model input, correction is needs to be perform. Multiplicative shift correction is useful to correct TRMM rainfall. **Figure 4.13** shows the corrected cumulative rainfall sample. Based on the evaporation temperature relationship, evaporation was also derived for individual catchments. The areas under different elevations of each sub-catchment have been computed by accumulating areas calculated for each incremental elevation using ASTER GDEM.

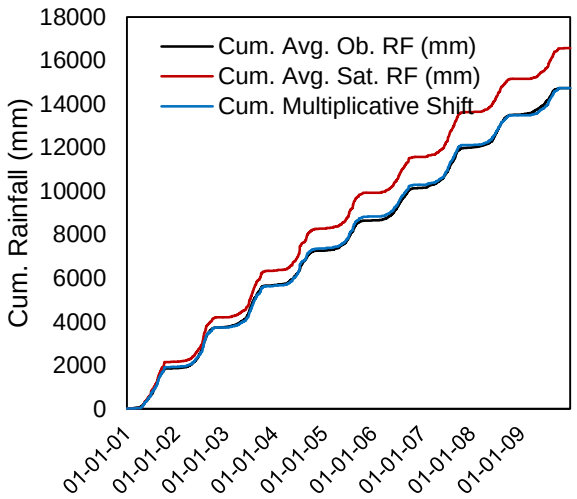

Figure 4.13: TRMM data correction sample plot

4.4.2.2 Temperature Estimation from MODIS Land Surface Temperature Data

MODIS Land surface temperature (LST) data is available with 1 km resolution. Ninsawat et al. (2010) illustrates a method to relate LST with observed ambient air temperature. Temperature data is very scarce in Himalayan range. Only two observed temperature station is available in the southern part of Koshi river basin (Okhaldhunga and Dhankuta, location in the Figure). Observed temperature data was collected for year 2013. MODIS LST data was correlate with observed data there was a missing data due to cloud cover.

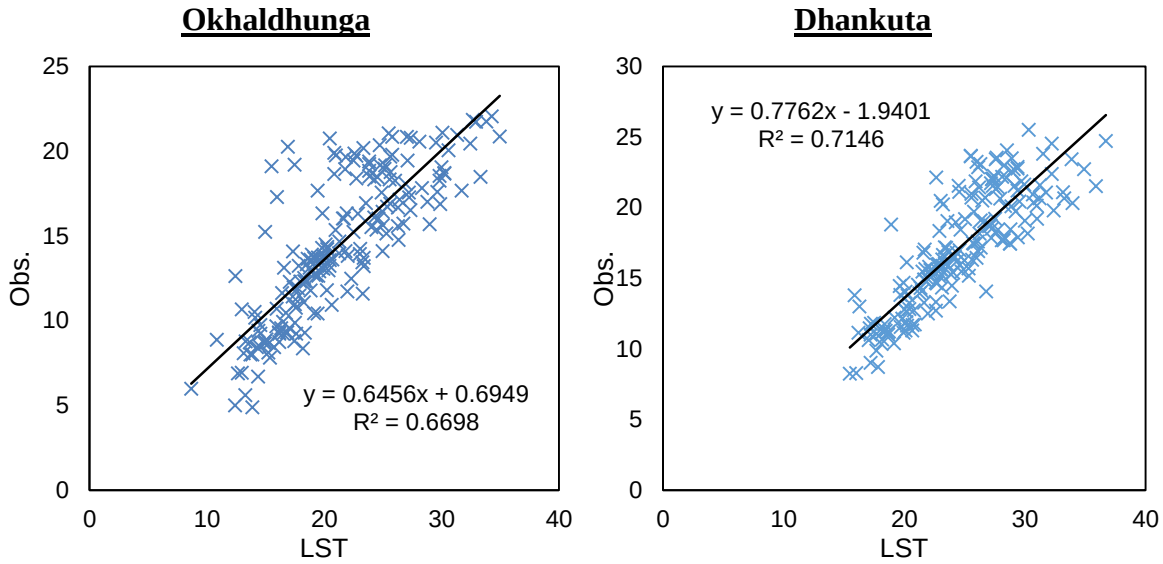

Figure: Scatter plot chart between MODIS LST and air temperature of Okhaldhunga and Dhankuta temperature station.

An average value for slope and intercept was used to estimate air temperature from LST. As an average temperature was used for individual catchment, LST data was collected for a number of location in that catchment to minimize the missing data.

	Slope	Intercept
Okhaldhunga	0.6456	0.6949
Dhankuta	0.7762	-1.9401
Average	0.7109	-0.6226

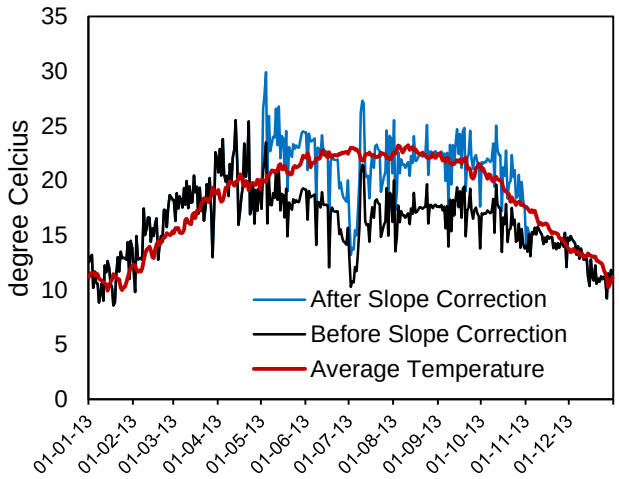

Figure 4.14: Temperature correction analysis

To handle missing data, a temperature model was developed using temperature data from Aphrodite from 2001- 2007 for the catchments separately. Model temperature is the mean daily temperature for 7 years. Climate change aspects were neglected here. Missing data can be predicted from previous 20 days of data after analyzing the temperature change pattern from temperature model data. Temperature change pattern was determined by using regression analysis. It is observed that for monsoon (May to October) about 60 – 88% data was missing for the year 2013 due to cloud cover. This missing data was replace by appropriate data after analyzing the trend of temperature model data (daily mean temperature form 2001 - 2007). Missing data replacement was led by slope and intercept correction based on average slope and intercept of Okhaldhunga and Dhankuta station. Corrected slope and intercepts are presented in the Appendix.

Temperature correction was based on the observed temperature in the south of the study area where elevation is comparatively low. Performing temperature estimation in the high elevated Himalayan mountain area in the northern part of the study area using MODIS LST

have some limitation of over estimation. Air temperature vs Land surface temperature ratio in the high elevation is lower than that of low elevation because of lapse rate. Using similar technique of correlating LST with air temperature, will always overestimate the air temperature in the high elevation.

4.4.2.3 Estimation of Evaporation using Temperature-Evaporation Correlation

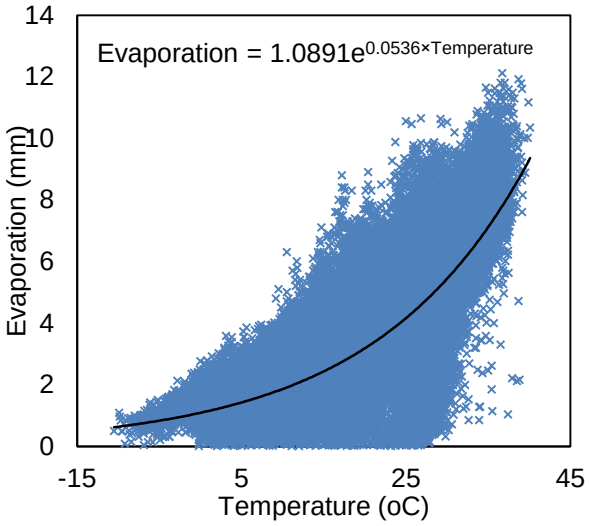

Figure 4.15: Evaporation vs Temperature correlation

Evaporation is dependent on various factors i.e. wind velocity, pressure, temperature, density etc. Nkemdirim (1991) develop a formula which is E = 0.45 exp (0.35 T + 0.025ū - 0.133 [e * - e]) yielded reasonable estimates of evaporation E is evaporation in mm/d, T, u and e *, e are temperature (°C), wind speed (m/s), saturation vapor pressure and vapor pressure (mb) respectively. For Koshi river basin, wind speed and vapor pressure information was unavailable. Here 41 gauge station was used to develop a statistical relationship between evaporation and temperature neglecting other factors. Here the formula is set to $E = 1.0891\ e^{(0.0536T)}$ where E = Evaporation (mm/d) and T = temperature (^oC).

4.4.3 Preparation of NAM Model Setup

The rainfall Runoff editor of MIKE 11 NAM model includes four sub menus for introducing parameters relevant to four different conceptual storage (surface storage, root zoon storage, groundwater storage and snow storage). In Koshi river basin Arun-2, Tamor-2 and Sun Koshi sub-catchment is not snow fed and rest is snow fed. For this reason these three sub-catchment was excluded from snow melt option. The surface storage includes seven parameters describing the topography, soil texture, land use and shape of the catchment. The groundwater parameters have been defined based on groundwater table record, soil characteristics and dry season catchment runoff record. Orographic phenomenon has been introduced in the hydrological model incorporating area-elevation relation of sub-catchments.

4.4.4 Calibration and Validation of Hydrological Model

The hydrological model has been simulated continuously from 2001 to 2007. The model has been calibrated based on secondary data. All record of meteorological as well as hydrological events are available in the form of either daily measure or daily averaged. The performance of model at different stations has been observed for the period 2001 to 2007. Time step of the model simulation has been considered as 1 hour. The validation of the model has also been checked for year 2007.

4.4.5 Error Indicator

The performance of the model is dependent on its capability to predict the flood peaks. The model flow should meet the peaks or exceed the observed flow during extreme events. According to IPCC, extreme event is defined as the 90 percentile flow. During the extreme event, model should reduce the number of days when simulated flow falls below observed flow. Based on the above assumption two parameters can be selected as performance indicator, which are-

(a) Number of days when model is under estimated during extreme event
(b) Average amount if under estimation during extreme event

Hydrological model was developed using Aphrodite gridded rainfall data and corrected TRMM rainfall data. To access the performance of the models, following objective function was used-

$$0.3\times (a) + 0.01\times (b)$$

4.5 HYDRO-DYNAMIC MODEL DEVELOPMENT

Hydrodynamic model has been developed using MIKE 11 Hydrodynamic (HD) module. The steps adopted in development of hydrodynamic model include: schematization of river system, preparation of river cross section database, preparation and defining boundary condition, calibration of model against measured data and validation.

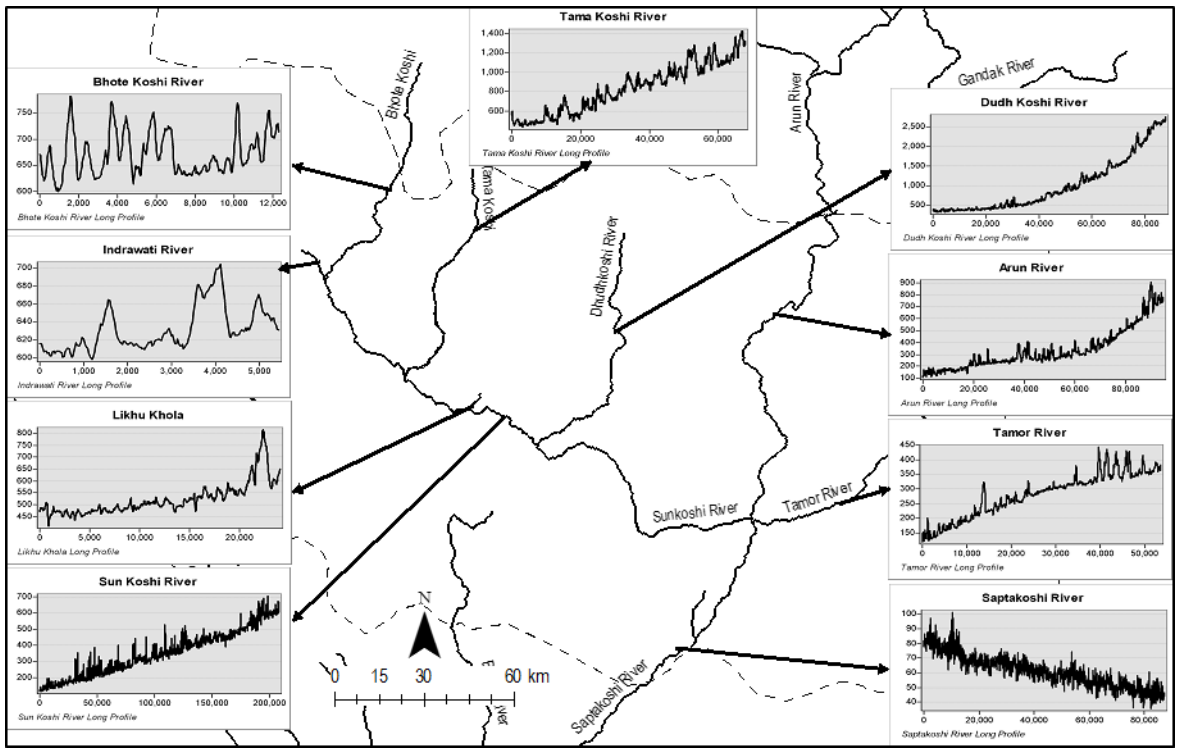

Figure 4.16: River long profile

4.5.1 Schematization of River System

MIKE 11 hydrodynamic module comprises the facilities to import geo-referenced GIS shape files for schematizing the river system. Also network can be digitized by keeping geo-referenced images in the background of network editor. The river network (**Figure 4.12**) of

the study area has been schematized by importing digital layer of alignment of rivers (GIS shape file) in the network editor of hydrodynamic module.

4.5.2 Preparation of Cross-section Database

Initially it was planned to extract cross section from SRTM 30 m resolution DEM. After data extraction, it was observed that extracted cross section is inconsistent and abrupt undulation was visible. Moreover it was realized that 30 m interval between two point in cross section is not representative cross section. This disadvantage lead to perform flow forecast. For flow forecasting, not actual cross section is required. Artificial cross section is sufficient to function as model input. Selection of artificial cross section maintain few consideration, which are-

- Cross-section size should contain the flow.
- Longitudinal slope (**Figure 4.16**) should be matched with river long profile.
- Downstream cross section should be larger than upstream cross section.

4.5.3 Definition of Boundary Condition

The upstream and downstream boundary points of the model have been placed at Arun-1 [Ch. 0], Indrawati [Ch. 0], Tamor-1 [Ch. 0], Likhu [Ch. 0], Dudhkoshi [Ch. 0] and Saptakoshi [Ch. 289000]. All the upstream rivers are snow fed and there is no inflow from another catchment. A minimum flow (10 m^3/s) was taken there. For the downstream there was no observed water level available. Downstream boundary station was selected almost 29 km away from interest point (Chatara) and a hypothetical water level was assumed after studying bed level. After the preliminary model run, it was make sure that downstream hypothetical water level does not affect Chatara result. Required adjustment was done to negate the downstream water level effect over Chatara simulation result. Estimation of river bed resistance roughness coefficient of the river is the most dominating calibration parameter for hydrodynamic model. In absence of such information, it has been assumed following the considerations stated by Chow (1959) which include composition and size of the bed material, degree of surface irregularity, variation of shape and size of river cross-sections, obstruction, vegetation and flow conditions and degree of meandering. River reach wise value have been optimized during calibration of model.

4.5.4 Calibration and Validation of Hydrodynamic Model

The hydrodynamic model has been calibrated against discharge using the data from 2001 to 2005. For this model there was no inflow and all flow comes from hydrologic model. During calibration, roughness coefficient (Manning's M) set initially has been tuned to within their limits until a satisfactory calibration achieved. The hydrodynamic model has been validate against discharge using the data for the period of 2005 to 2007. The performance of the model has been observed by comparing model simulated discharge against available measured discharge.

4.6 FLOOD FORECAST MODEL DEVELOPMENT

Flood forecasting model has been developed using MIKE 11 flood forecasting (FF) module. The steps adopted in development of flood forecasting model include: Rainfall Forecasting, Hindcast and forecast period, real time updating.

4.6.1 Rainfall Forecasting

Flood forecasting is vastly dependent on rainfall forecasting. Rainfall forecasting information normally comes from different Weather Research and Forecasting (WRF) Model of different agencies. NCEP provides GFS model output for 8 days in 3 hour interval. The data is available in gridded binary (.grib) format. Data is available in 0.5^o resolution. Rainfall forecast data is available as surface precipitation rate (6 hour average) in $kg.m^{-2}s^{-1}$ or mm/s unit. After some processing, data is available as accumulated rainfall for 6 hour in mm in grid format. After performing Thiessen polygon analysis, catchment average rainfall forecast data is ready to use. ECMWF requires similar processing. This data is available both in netCDF and .grib format, 0.75^o resolution and with 6 hour interval.

To test the flood forecasting model validity, another set of rainfall forecasting data was prepared using actual rainfall.

4.6.2 Hindcast and Forecast Period

Hindcast period is known as closely estimated inputs for past events which are entered into the model to train output. Forecast is dependent on hindcast. Closely matched hindcast leads to more accurate forecast. There is no indication of taking certain range of hindcast period. For this flood forecasting maximum available hindcast period was selected based on availability of data.

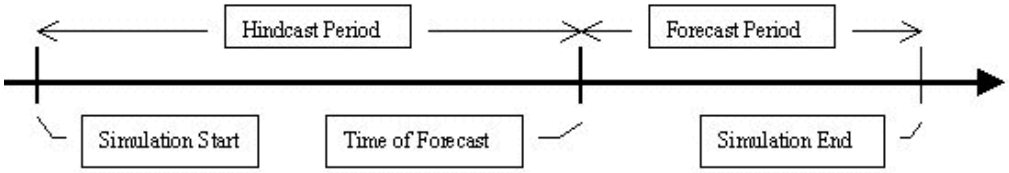

Figure 4.17: Hindcast and Forecast Period

4.6.3 Real Time Updating

Real time updating in flood forecasting is used to execute simulations by applying real-time hydro-meteorological data. Real-time hydrological and meteorological data are often captured and supplied by a telemetry network.

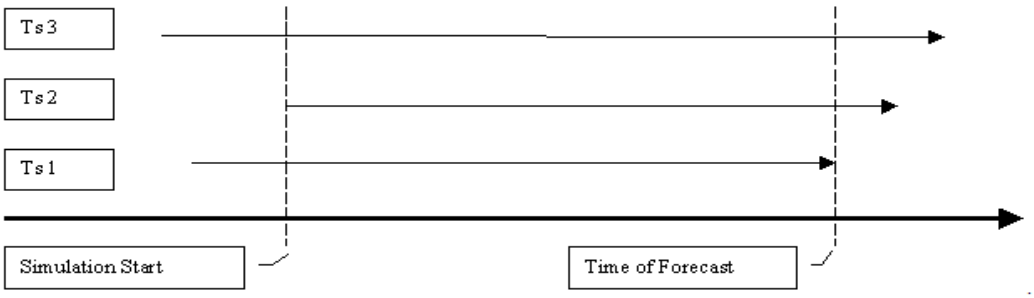

Figure 4.18: Real-time updating

The purpose of updating is to evaluate and eliminate deviations between observed and simulated data in the hindcast period to improve the accuracy of the model results in the forecast period. Phase and amplitude errors are identified by the updating routine and corrections in the hindcast and the forecast period are subsequently applied. Remote sensed flow estimation or telemetric flow measurement of DHM has a potential to provide real-time flow information and also update the flood forecasting model result to improve the forecast.

4.6.4 Forecasting Lead Time

Forecast lead time is the minimum period of advance warning necessary for preparatory action to be taken effectively. In the case that telemetric rain gauge data or radar rainfall information are available, forecast can be presented as input suitable for the catchment forecast model, several hours may be added to the flow-forecast lead time (WMO, 2011). Similar study has been done for Baghmati River basin in Nepal where flood forecasting has 3 day lead time (Shah-Newaz & Magumdar, 2011). For this research 6 days of flow forecasting was examined.

4.6.5 Estimation of Accuracy

Flood forecast data should closely match with actual flow. Under estimated flow is not good forecasting. Overestimated flow is not good forecasting as well, because it will create a false result of forecasting. Forecast deviation from extreme event can be accessed by peak error. Peak error could be defined as-

$$\text{Peak Error} = \frac{Simulated\ Flow - Observed\ Flow}{Observed\ Flow}\ \%$$

Here positive peak error indicates overestimation and negative peak error indicates under estimation. Extreme event could be denoted as 90 percentile of the flow.

CHAPTER 5
RESULT AND DISCUSSION

5.1 FLOW ESTIMATION USING REMOTE SENSING

Flow estimation using remote sensing was done using two different approaches which are (1) microwave approach and (2) water surface reflectance approach.

5.1.1 Microwave approach for Flow Estimation

Microwave approach technique for flow estimation was tested for several stations namely Akardh (86.43°E; 25.95°N) India, Farakka (88.065°E; 24.614°N) India Chilmari (89.775°E; 25.514°N) Bangladesh, Chatara (87.14°E; 26.87°N) Nepal and Kushaha (87.01°E; 26.63°N) Nepal. Using the Flood Signal tool (**Appendix-1**), flood signal was generated for the aforementioned stations. Observed data at Chatara was available from DHM and observed data at Akardh, Farakka and Chilmari was available from discharge achieve of DFO. Comparison of the estimated flow and observed flow are presented below-

Figure 5.1: Testing location

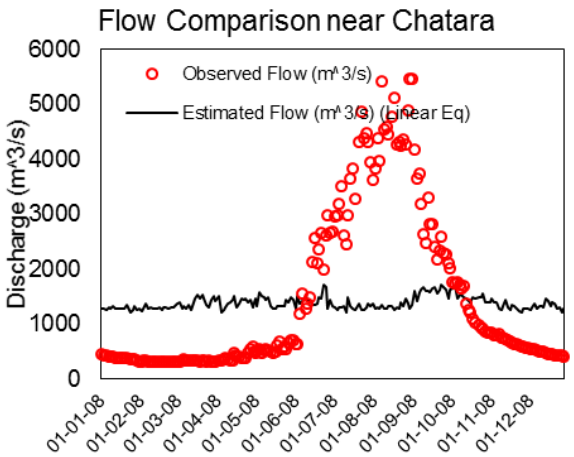

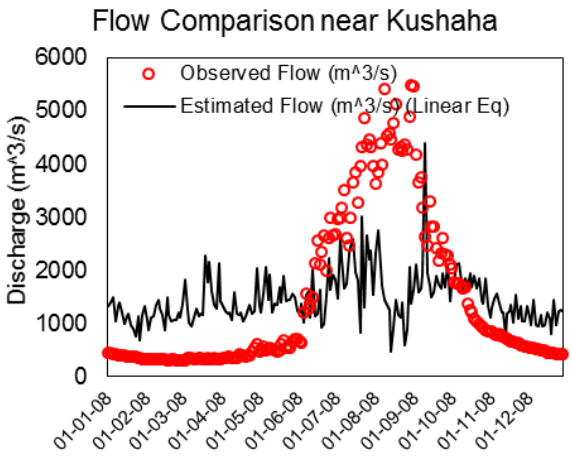

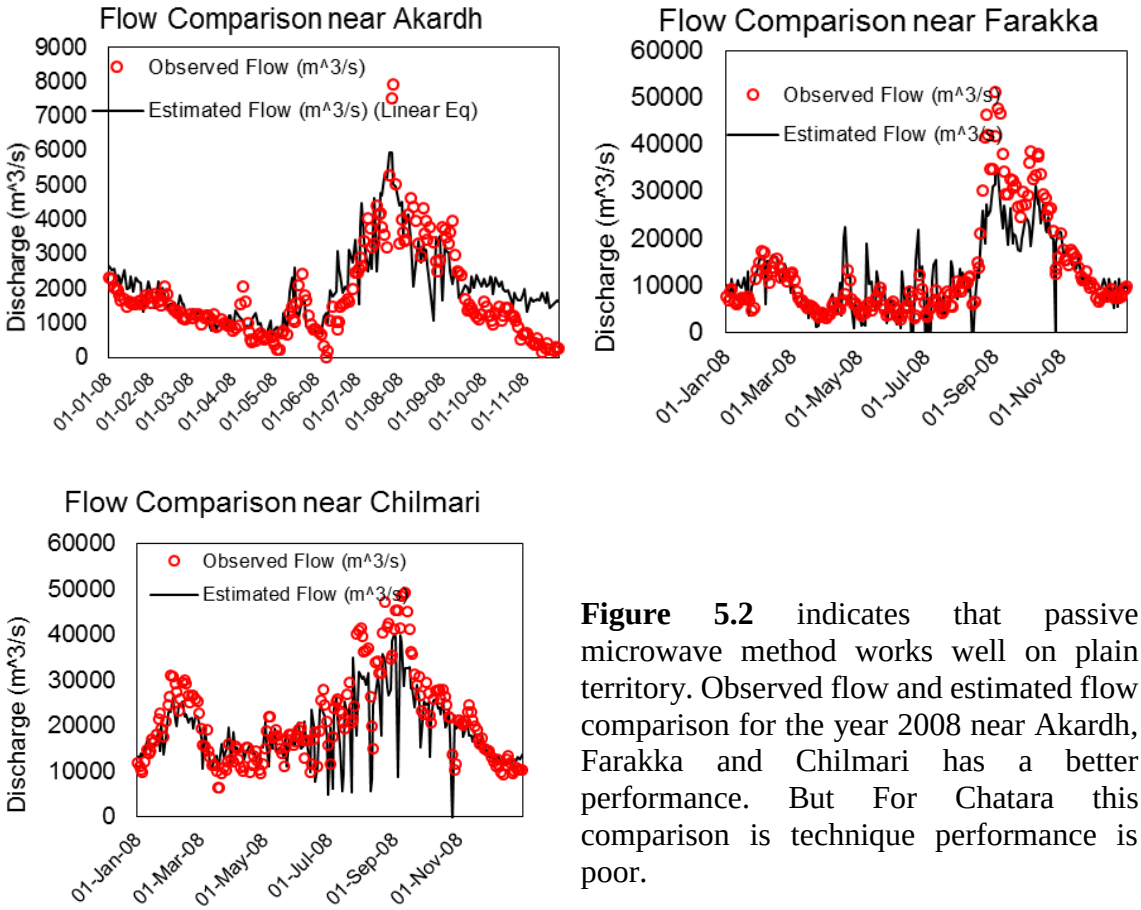

Figure 5.2: Flow comparison result

Figure 5.2 indicates that passive microwave method works well on plain territory. Observed flow and estimated flow comparison for the year 2008 near Akardh, Farakka and Chilmari has a better performance. But For Chatara this comparison is technique performance is poor.

Table 5.1: Error estimation for flow estimation using microwave approach

	Chatara	Kushaha	Akardh	Farakka	Chilmari
EI	1.0%	13.7%	50.3%	68.5%	52.1%
RMSE	1449.4	1365.3	923.1	6027.5	6724.5
R	11.1%	37.3%	77.9%	84.4%	76.0%

After performing slope analysis, it is observed that the slope of Akardh (0.0092 m/km or 0.000527^{o}) is the initial slope. So, microwave approach for estimation is valid for the terrain which has a slope of 0.0092 m/km or 0.00527^{o} or lower. Koshi river basin has a higher terrain slope which leads to water surface reflectance approach for flow estimation.

5.2 WATER SURFACE REFLECTANCE APPROACH FOR FLOW ESTIMATION

LANDSAT (L-8 OLI/TIMR) data was used for model training purpose at Chatara station. L-8 is available from February 2013, so only 5 cloud free image (14-Jan-14, 27-Nov-13, 11-Nov-13, 26-Oct-13 and 24-Sep-13) was available for data training. Using the water surface reflectance formula the log ratio of water surface reflectance was correlated with observed flow. Detain table is provided in Appendix. Observed data was acquired from DHM. Here data training was performed for two stations namely Chatara and Mulghat. For Mukghat station 6 images of LANDSAT-7 (L-7 ETM+ SLC off) used from 2001 to 2007.

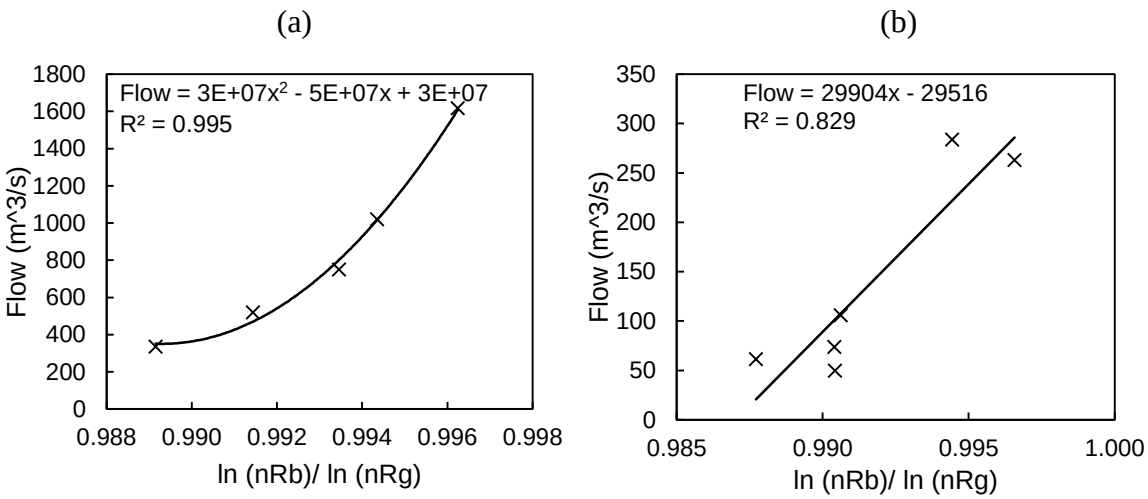

Figure 5.3: Data training for (a) Chatara and (b) Mulghat Station

Data testing was performed at Chatara station using 6 images of LANDSAT-7 (L-7 ETM+ SLC off) used from 2001 to 2007. Model is appeared to be acceptable for higher flow. Error is high for low flow simulation. This high error was influenced by many factors i.e. sediment load in the river, haze over area etc.

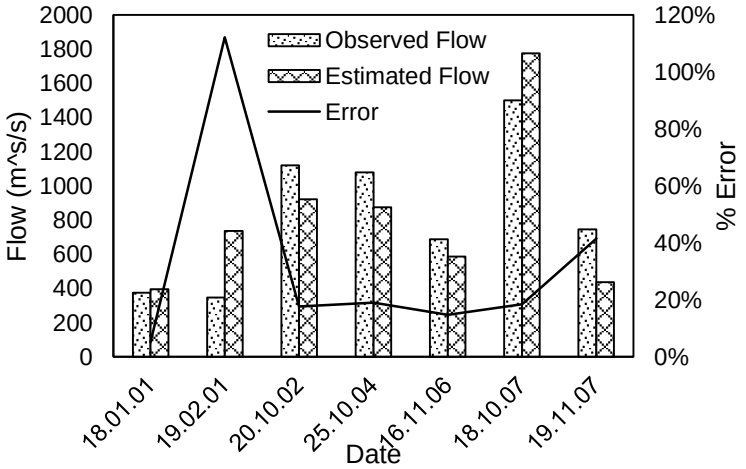

Figure 5.4: Data testing at Chatara Station

For data training and testing purpose, very few images were available to work on. It is because LANDSAT does not provide daily data. It provides 2 images in one month. And moreover for the monsoon period, area is often covered with cloud, which was not useful for data extraction. MODIS surface reflectance data is provided in daily basis, but that image is not suitable, as its resolution is coarse.

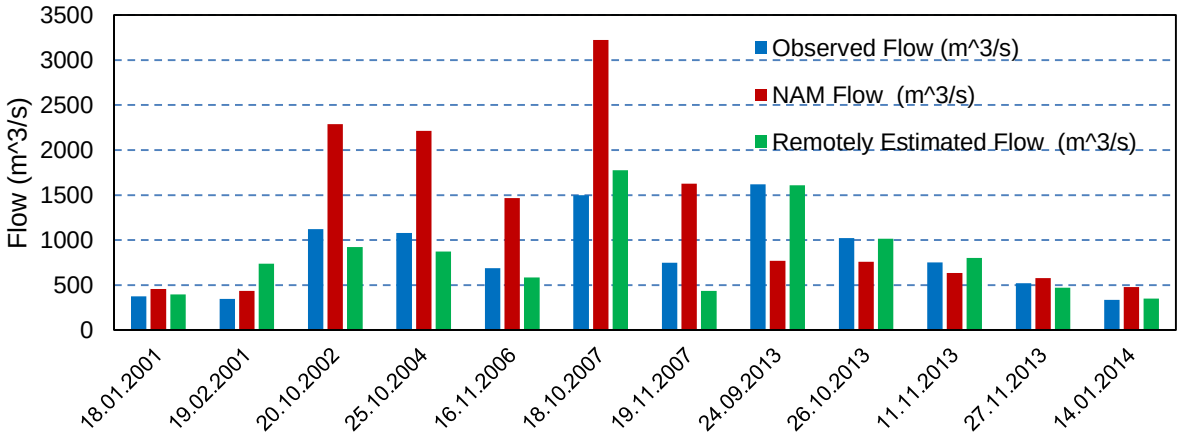

Figure 5.5: Comparison of flow estimated from different methods at Chatara

A comparison plot was prepared among the observed flow, flow from hydrological (NAM) model and estimated flow using remote sensing at Chatara station. As NAM model was over estimated, it exceeds most of the flow. Observed flow and estimated flow appears closely.

This technique was developed to update flood forecasting model in real time. But at present, LANDSAT images are not available in daily basis. NASA is going to launch a LANDSAT constellation project by launching few more satellite in space(Ramachandran, Justice, & Abrams, 2010). This will increase the availability of image more frequently and possibility will also increase to acquire an image in monsoon season. This developed technique has a potential to generate flow time series when images can be acquired more frequently.

5.2 DATA PROCESSING AND ANALYSIS

Data consistency check has been conducted using standard data processing methods.

5.2.1 Rainfall Data

Daily rainfall data at 76 TRMM pixel for the period 2001 to 2010 has been extracted from TOVAS website. The rainfall records were found to be consistent after double mass analysis. In some case TRMM rainfall does not match with observed data. Correction need to be done before use as model input. Aphrodite precipitation data was downloaded and extracted exactly same location with TRMM station and multiplicative shift correction was done.

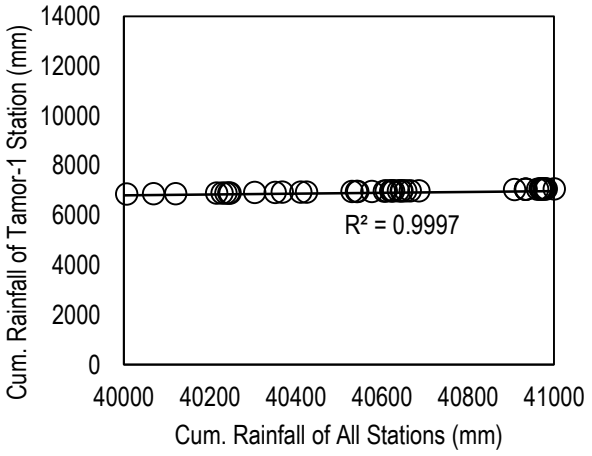

Figure 5.6: A sample plot of double-mass analysis of rainfall data

5.2.2 Temperature

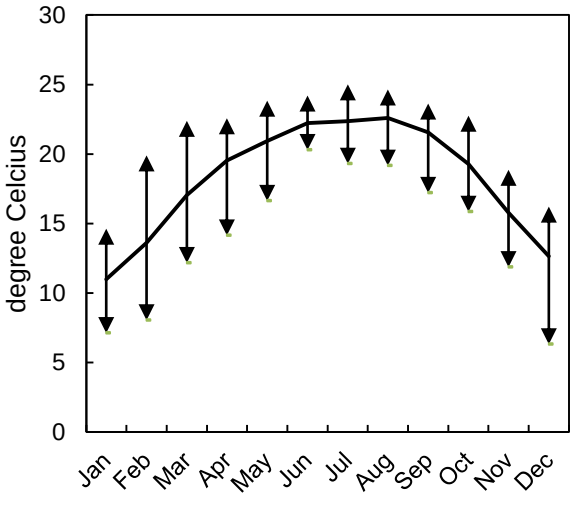

Figure 5.7: mean monthly variation of temperature

Temperature data was downloaded from 60pixel of 25km×25km from Aphrodite website. Data was available from 2001 to 2007. After necessary quality checking, processed data for the period of 2001- 2007 have been included in the model. For the temperature after 2007, MODIS Land surface temperature (LST) data was acquired (MOD11A1). A correlation between LST and observed temperature was established to estimate air temperature properly. From the available record it is observed that monthly temperature in the basin area temperature variation is high

(maximum 28 ^{o}C, minimum -18.7^{o}C). In the southern part where elevation is below 2,000 m, temperature varies from 1 – 28 ^{o}C. Sample plot showing mean monthly variation of temperature at No. 58 TRMM station is given in **Figure 5.8**.

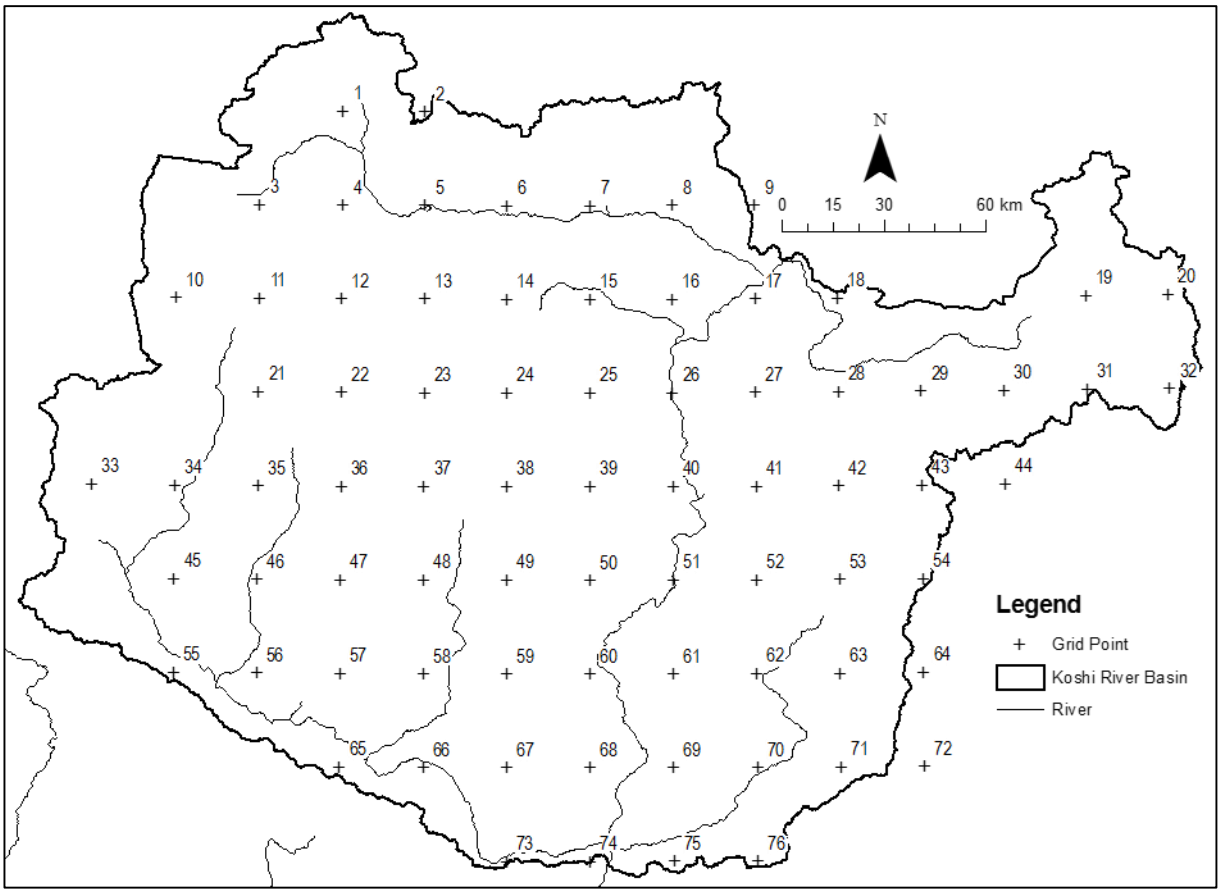

Figure 5.8: TRMM Rainfall Station Location

5.2.3 Evaporation Data

Primary evapotranspiration data was collected for different projects of ICIMOD. After collection, data was processed for the Koshi basin. There was no observed data available to cross check it. Temperature is one of the factor for evaporation. Evaporation was correlate with temperature using different station observed temperature and evaporation data. Evaporation data was derived from the temperature- evaporation relation. Evaporation value varies from 0.58 mm/day to 4.45 mm/day in Koshi River basin.

5.2.4 Water Level and Discharge

Historical discharge data of Mulghat on Tamor, Turkeghat, Simle on Arun, Hampuachwar, Khurkhot on Sun Koshi have been collected, processed and analyzed. Data was available from 2001 to 2007 with some missing data. Historical discharge records at every stations have been plotted to check their consistency. Water level data was unavailable. Necessary quality checking and analysis of these data has been carried out including plotting data, comparing with upstream and downstream station, response of catchment rainfall.

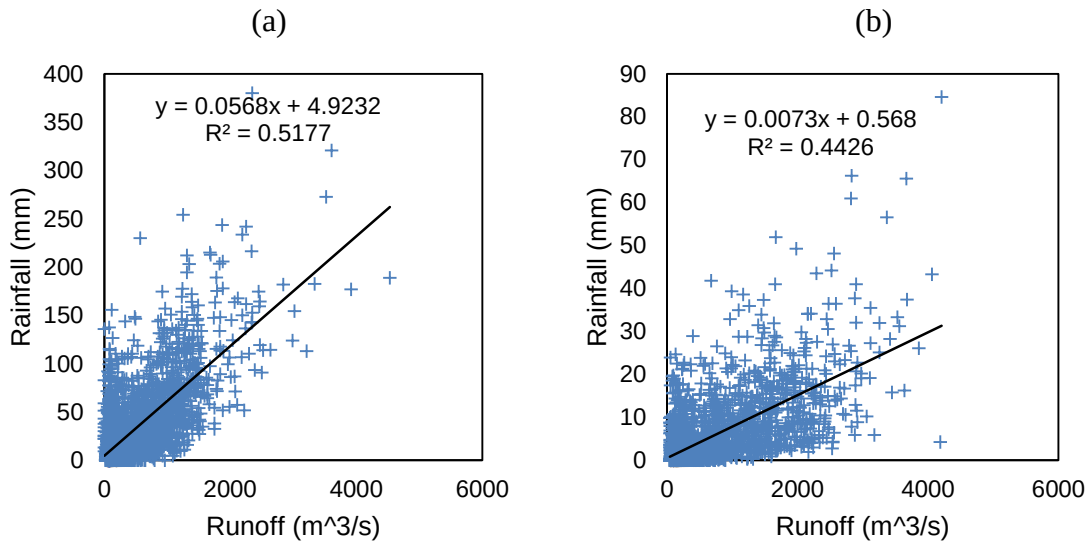

Figure 5.9: Rainfall-Runoff relationships (a) Mulghat from 2001-2007 (b) Khurkot from 2001-2007

5.2.5 Groundwater

Groundwater data from secondary source was available from ICIMOD. Model parameters were taken from study area portion of GBM basin model.

5.2.6 River Cross-section

As no measured cross sections were available, cross section was taken from ASTER DEM using 3D analyst tool of ArcGIS 10.1 for all the channels in this basin. Longitudinal bed slope were maintained in the cross section.

5.2.7 Rainfall Forecast

Rainfall forecast data was available from Global Forecast System (GFS) model of National Center for Environmental Prediction (NCEP) and European Centre for Medium Range Weather Forecasts (ECMWF). GFS forecast data is available in .grib format and with 0.5° resolution. ECMWF data is available in both .grib and netCDF format with 0.563° resolution. NASA provided freeware Panoply 3.2.1 was used to extract the data.

5.3 HYDROLOGICAL MODEL OF KOSHI BASIN

The hydrological model has been developed using MIKE 11 NAM (rainfall-runoff) module developed by Danish Hydraulic Institute (DHI). The NAM is deterministic, lump and conceptual model. Hydrological model developed for the Koshi river basin comprises 10 catchments (**Table 5.2, Figure 5.10**). All the catchments are located in Tibetan Himalaya, higher Himalaya, lesser Himalaya, siwalik and terai region. The sub-catchments use TRMM rainfall. Average rainfall for individual catchments were determined after Thiessen polygon analysis.

Table 5.2: List of NAM Sub-Catchment and corresponding Areas

Name	Outlet Hydrological Station	Area (km^2)	Drains to river
Arun-1	Turkeghat	25,342.92	-
Bhote Koshi		3,612.62	Sun Koshi
Indrawati		1,228.98	Sun Koshi

Name	Outlet Hydrological Station	Area (km^2)	Drains to river
Tama Koshi	Khurkot	5,345.34	Sun Koshi
Dudh Koshi		4,066.94	Sun Koshi
Likhu		1,051.35	Sun Koshi
Sun Koshi	Hampuachuwar	2,840.99	Saptakoshi
Tamor-1	Mulghat	5,892.25	-
Arun-2	Simle	2,288.32	Saptakoshi
Tamor-2	Chatara	225.28	Saptakoshi

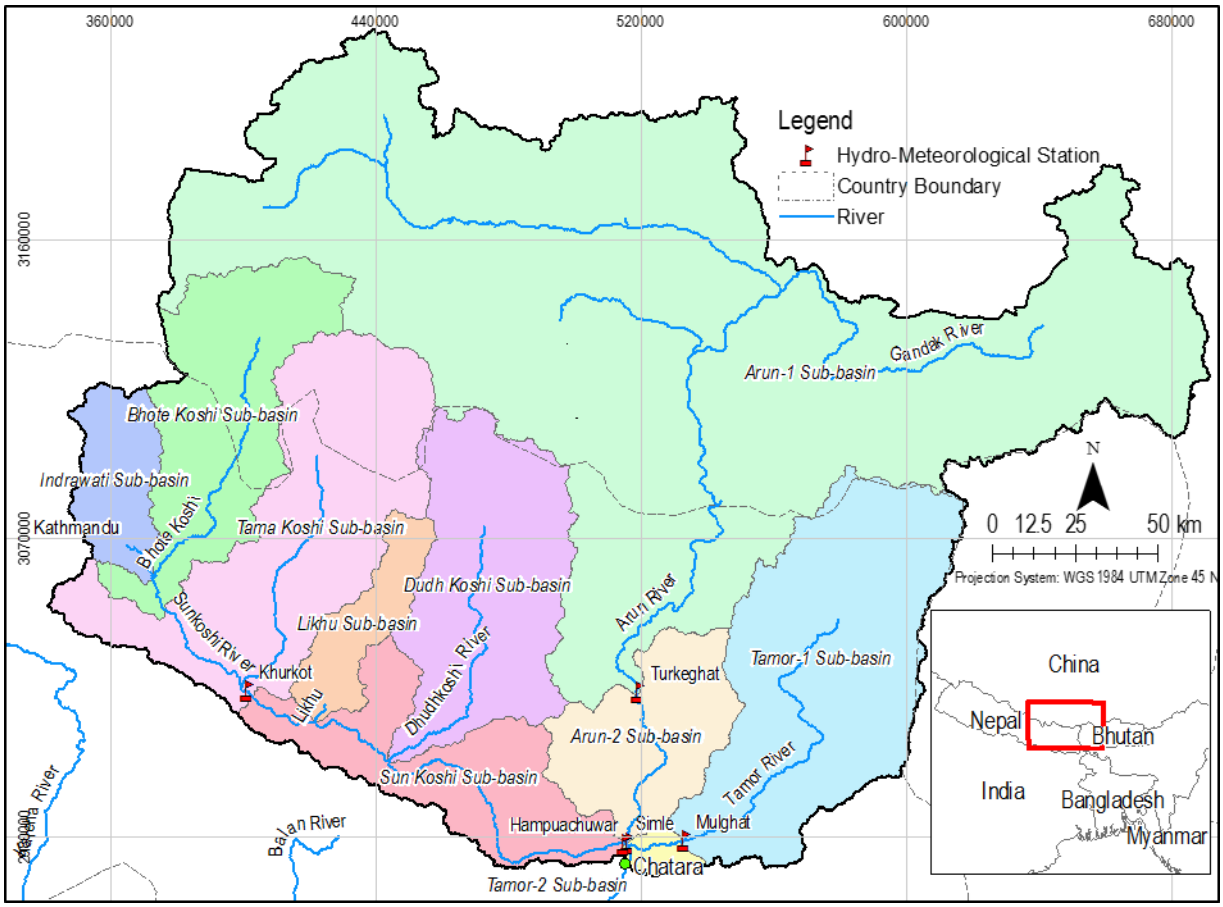

Figure 5.10: Sub-catchments of hydrological model of the Koshi river basin

The area-elevation curves of sub-catchments are given in **Figure 5.10**.

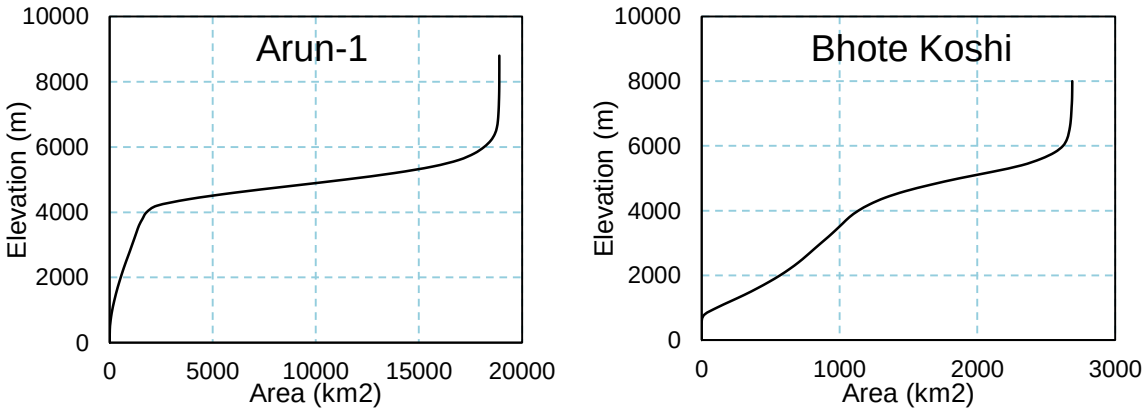

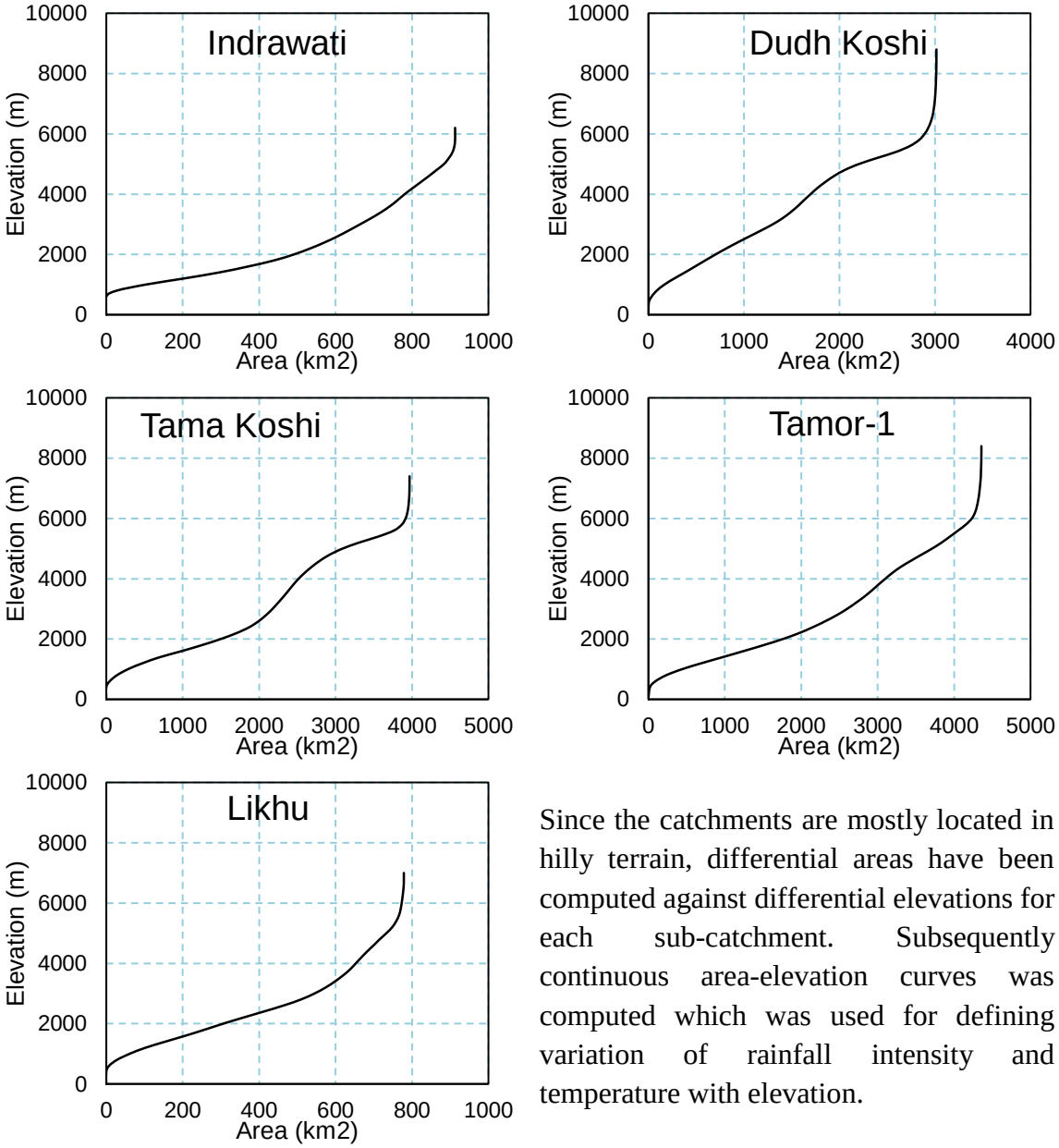

Figure 5.11: Area-Elevation curve for different sub-catchments

Since the catchments are mostly located in hilly terrain, differential areas have been computed against differential elevations for each sub-catchment. Subsequently continuous area-elevation curves was computed which was used for defining variation of rainfall intensity and temperature with elevation.

In order to account for the large variations in precipitation and temperature with altitude, the reference series was adjusted for each altitude zone. This adjustment was done for the effect of lapse rate and local factor. In this catchments lapse rate was 0.5 ^{o}C/100 m. Correction in temperature and precipitation was done due to inconsistency of model outcome. When temperature and precipitation seem unlikely for a zone, correction takes place instead of actual value.

The hydrological model was calibrated based on discharge data. All records were available in the form of daily data. Time step of the model simulation was considered to be 1 hour because the catchment area is mountainous where runoff from rainfall takes place within a very short time. Calibrated values of NAM parameters are given in **Table 5.3**. Calibration was done against available discharge at 7 stations.

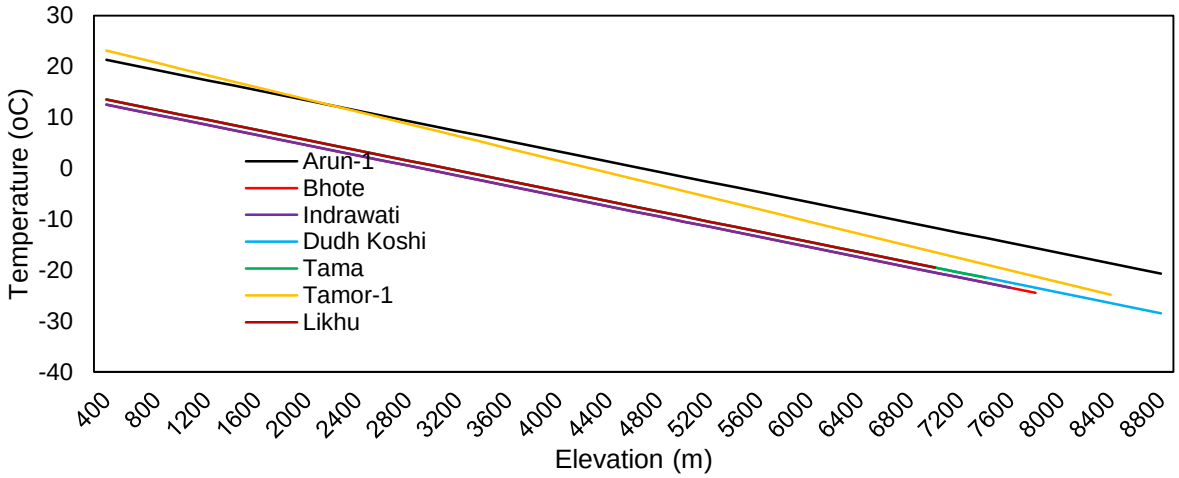

Figure 5.12: Temperature Correction

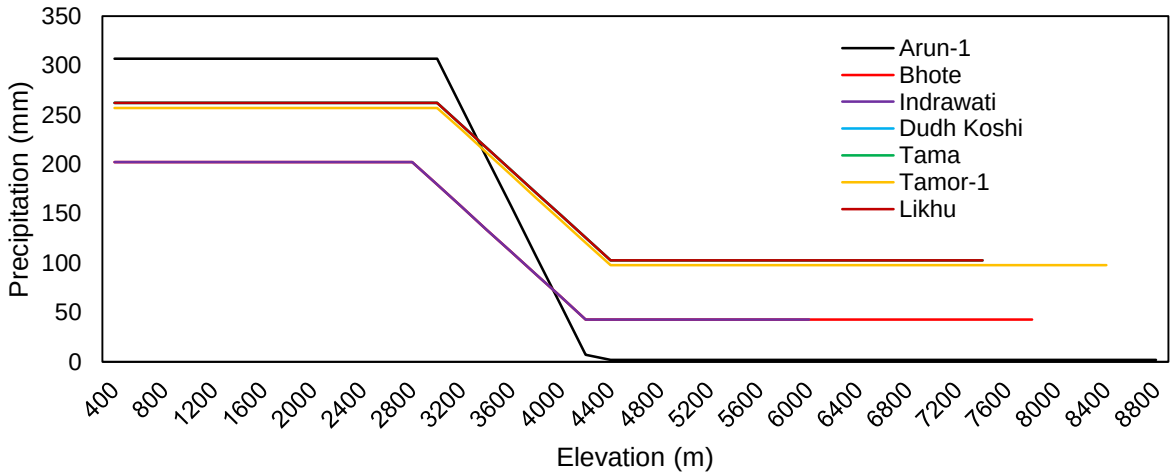

Figure 5.13: Precipitation Correction

Table 5.3: Values of Calibrated NAM Parameters

Storage Zone	Parameter	Elaboration	Values Used	Typical Value
Surface-Rootzone	U_{max}	Maximum water content in surface storage	10.0-40.0	10-20 mm
	L_{max}	Maximum water content in root zone storage	25-300	50-300 mm
	CQOF	Overland flow runoff coefficient	0.1-1	0-1
	CKIF	Time constant for interflow	150-1000	500-1000 hr.
	CK1	Time constants for routing overland flow	5.0-75.0	3-48 hr.
	CK2		10.0-50.0	-
	TOF	Root zone threshold value for overland flow	0-0.99	0-0.7
	TIF	Root zone threshold value for inter flow	0-0.99	-
Groundwater	TG	Root zone threshold value for ground water recharge	0-0.99	0-0.7
	CKBF	Time constant for routing baseflow	500-4000	-

Storage Zone	Parameter	Elaboration	Values Used	Typical Value
	C_{area}	Ratio of ground water catchment to topographical (surface water) catchment area	1	-
	S_y	Specific yield for the ground water storage	0.1	0.01-0.3
	GWLBF0	Maximum ground water depth causing baseflow	10	-
	GWLBF1	Depth for unit capillary flux	0	-
	CQLOW	Lower base flow. Recharge to lower reservoir	1-100	-
	CKLOW	Time constant for routing lower baseflow	1000-30000	-
Snow Melt	C_{snow}	Degree-day coefficient	2	2-4 mm/day/^oC
	T0	Base Temperature	0	0^oC

5.3.1 Calibration and Validation

The following figures indicates the calibration and validation of the NAM model with respect to the river flow.

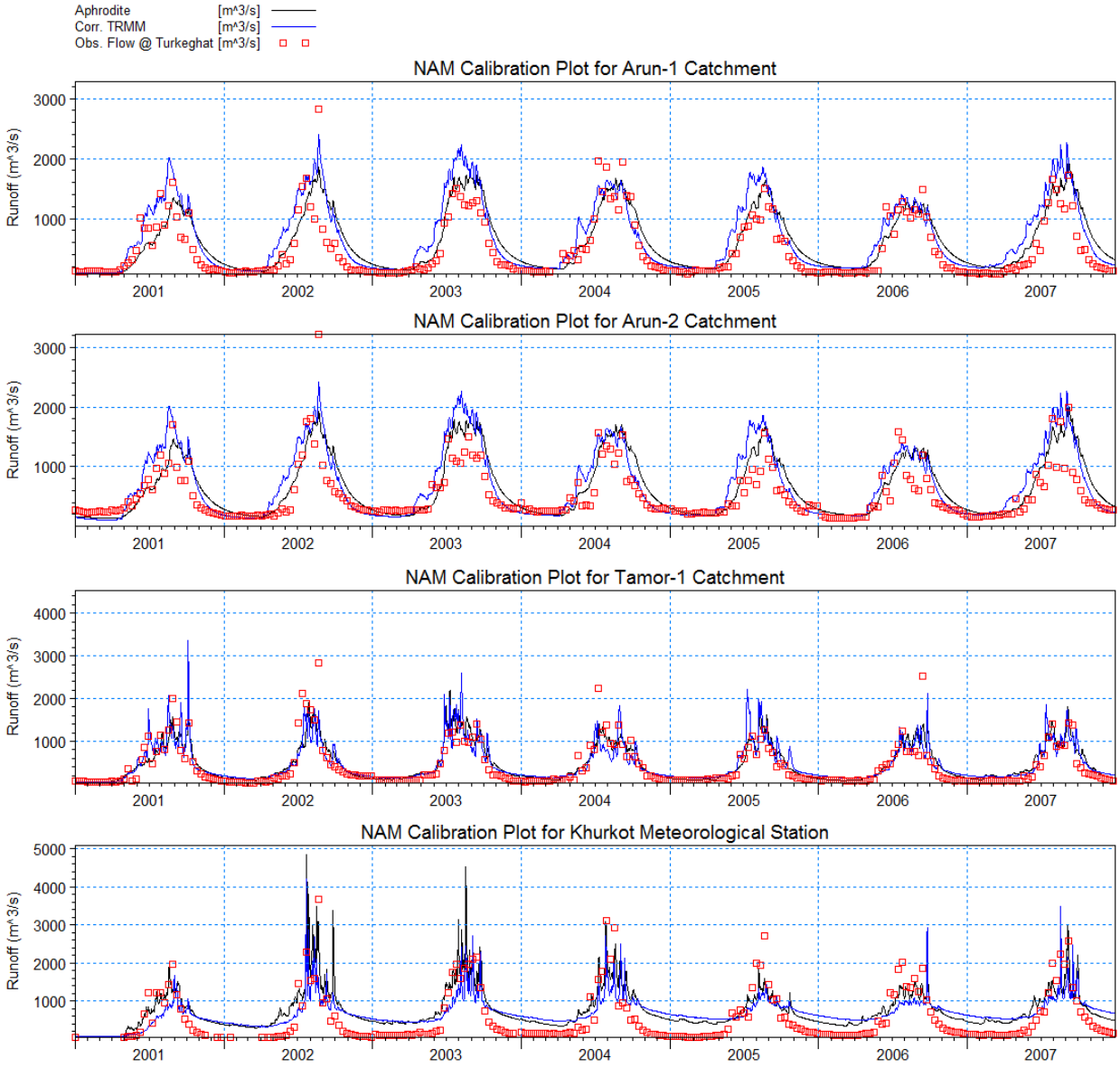

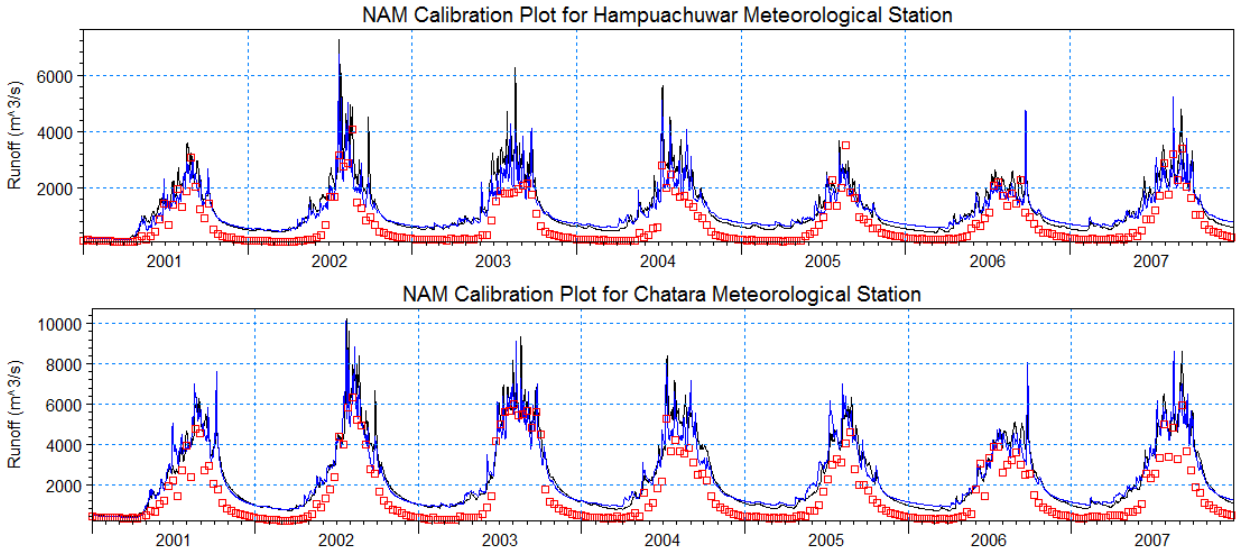

Figure 5.14: Calibration and Validation plots of hydrological model against discharge

5.3.2 Model Performance

Model performance depends on the number of days when model is under estimated during extreme event and average amount of under estimation during extreme event. Here lower value indicates the more acceptable model. **Figure 5.9** indicates the model performance for different stations. Being in the downstream of the entire basin, Chatara poses as an important station. For this reason, to determine the overall indicator over the basin area, Chatara station indicator was given 50% weightage. After the calculation (**Table 5.4**) it is observed that model using Aphrodite rainfall data is acceptable.

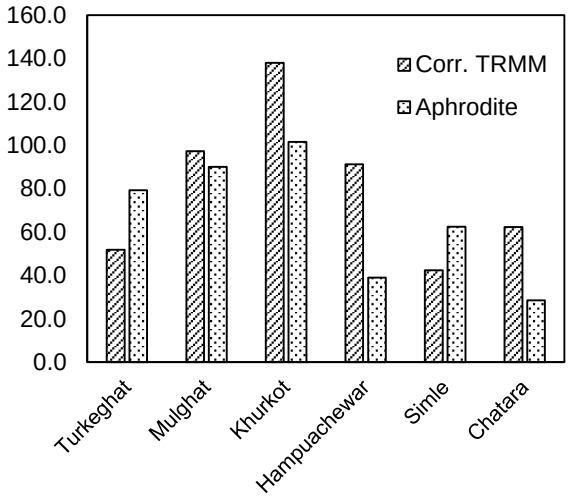

Figure 5.15: Model performance indicator for different stations

Table 5.4: Model Performance Indicator

Model	Turke ghat	Mul ghat	Khur-kot	Hampua chewar	Simle	Chatara	Overall Indicator
Corr. TRMM rainfall	51.8	97.3	138.0	91.2	42.3	62.3	73.2
Aphrodite rainfall	79.3	90.0	101.5	39.0	62.4	28.5	**51.5**

5.4 HYDRODYNAMIC MODEL OF KOSHI BASIN

The hydrodynamic model was developed using hydrodynamic (HD) module of MIKE 11 developed by Danish Hydraulic Institute (DHI). The HD module computes steady and unsteady flows also capable to describe sub-critical and supercritical flow conditions. Hydraulic model of the Koshi river basin includes 117 km reach of Arun River, 289 km reach of Saptakoshi River, 12.4 km reach of Bhote Koshi River, 5.25 km reach of Indrawati River, 23.7 km reach of Tamakoshi River, 6.5 km reach of Likhu Khola, 211 km reach of

Sun Koshi River, 24 km reach of Dudh Koshi River and 51.5 km reach of Tamor River. The model comprises of 57 remotely extracted cross section. Upper boundary inflow was taken at Arun-1 [Ch. 0], Indrawati [Ch. 0], Tamor-1 [Ch. 0], Likhu [Ch. 0] and Dudhkoshi [Ch. 0].

As there is no actual inflow in these rivers rather than the rainfall runoff, so minimum inflow was given as model input [10 m^3/s]. Saptakoshi [Ch. 289000] was taken as downstream boundary. As no water level was available there, so a carefully estimated water level [44 m] was given as model input there. After the model run, it was ensured that this assumed water level did not affect the result of 289 km upstream interest point [Chatara].

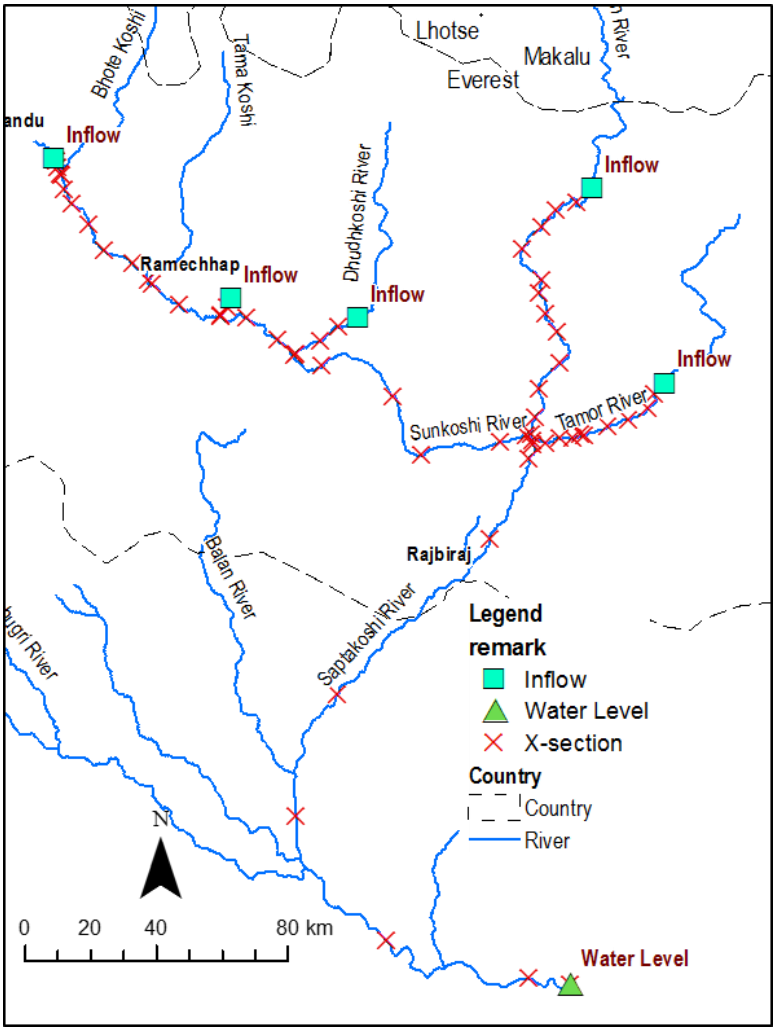

Figure 5.16: River System and boundary stations of hydrodynamic model

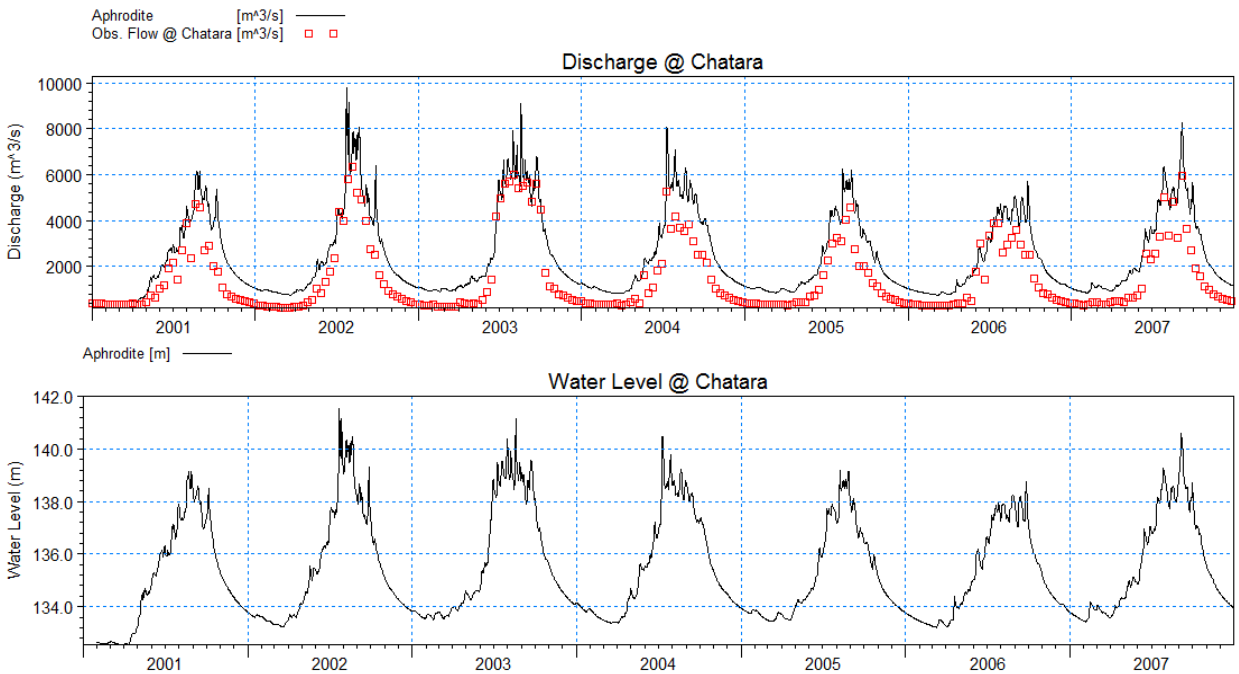

Figure 5.17: Calibration and validation for HD model at Chatara [Saptakoshi 625.00]

The hydrodynamic model was calibrated against discharge from 2001-2007 in 6 stations namely Turkeghat, Mulghat, Simle, Hampuachewar, Khurkot and Chatara. Manning's M was used as 30. Calibration and validation plot shows that, HD result does not vary with NAM results. This is the effect of having no inflow here.

5.5 FLOOD FORECASTIN MODEL OF KOSHI BASIN

The flood forecasting model has been developed using MIKE 11 flood forecasting (FF) module developed by Danish Hydraulic Institute (DHI). Due to unavailability of actual measured river cross section and observed water level data, only flow forecasting was possible. FF model is designed to perform calculations to predict the flow from catchment rainfall and inflow, outflow in the catchments. This forecasting is not facilitate with real-time flow updating. Several cases were studied to assess the accuracy of the FF model. These are-

Case-1	TOF 21-07-2002 6 day forecast Observed Rainfall as forecast data and ECMWF rainfall forecast data
Case-2	TOF 24-06-2013 6 day forecast GFS & ECMWF Rainfall forecast data
Case-3	TOF 26-05-2013 6 day forecast GFS & ECMWF rainfall forecast data
Case-4	TOF 22-03-2014 6 day forecast GFS & ECMWF rainfall forecast data

5.5.1 Case-1: Monsoon 2002

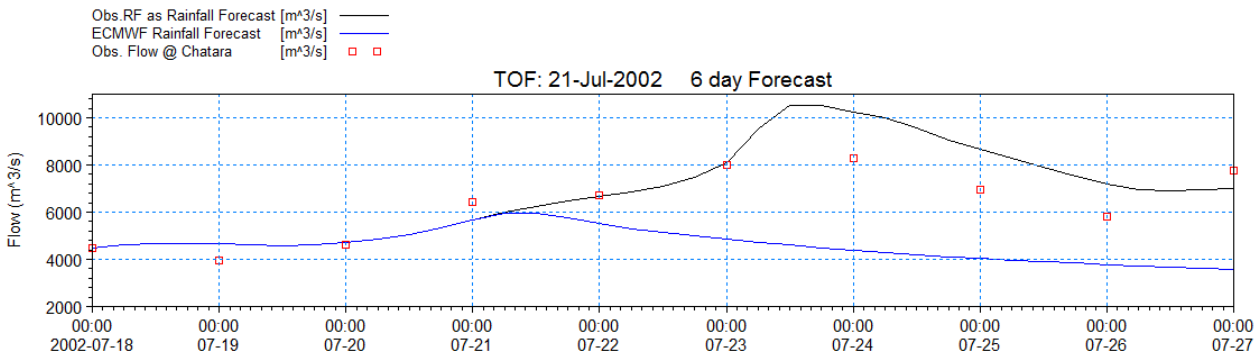

This case was taken in between the model calibration period (2001-2005). The purpose of taking this time period is to assess the accuracy of the FF model for historical data and also with observed rainfall data. Result follows actual calibration plot. GFS rainfall forecast data was unavailable for that period. ECMWF

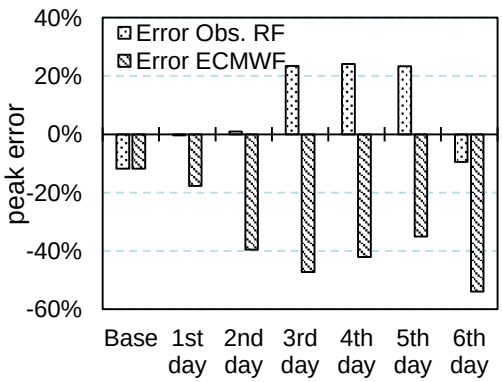

5.5.2 Case-2: Monsoon 2013

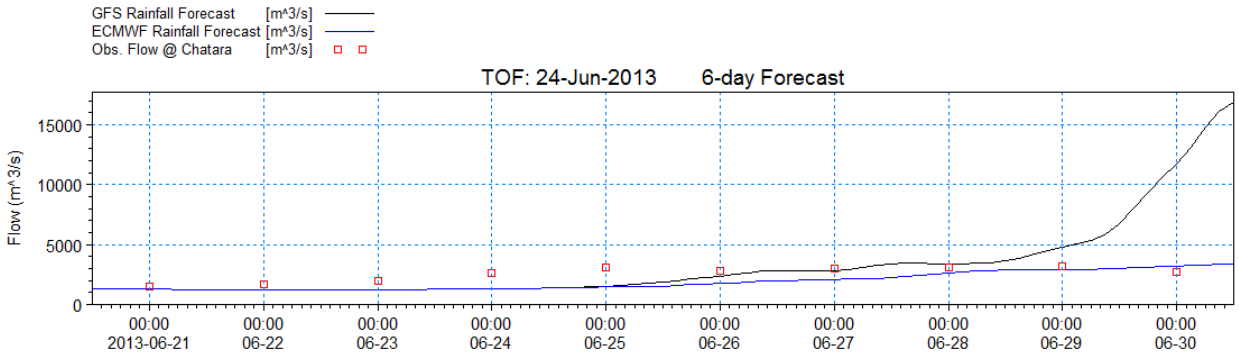

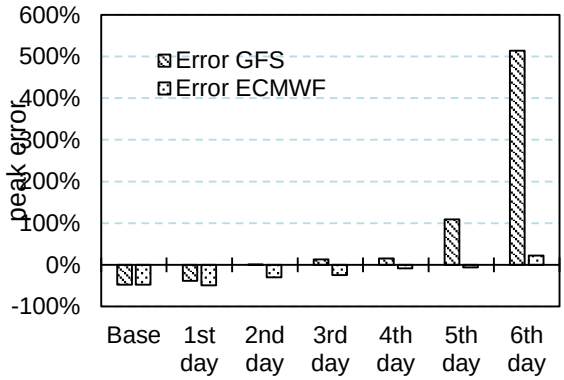

This case was taken in the latest monsoon peak time period (June 2013). The purpose of taking this time period is to assess the accuracy of the FF model for recent peak flow. Data training in the end of hindcast (from 22-06-13 to 24-06-13) period appears deviated from actual flow. This deviation affects forecasting. Flood forecasting using GFS rainfall forecast data is lagged by 1 day and after 4 day forecasting is not acceptable limit. Flood forecasting using ECMWF rainfall forecast data is lagged by 4 days. GFS forecasting data is proves more appropriate for this case.

5.5.3 Case-3: Pre-monsoon 2013

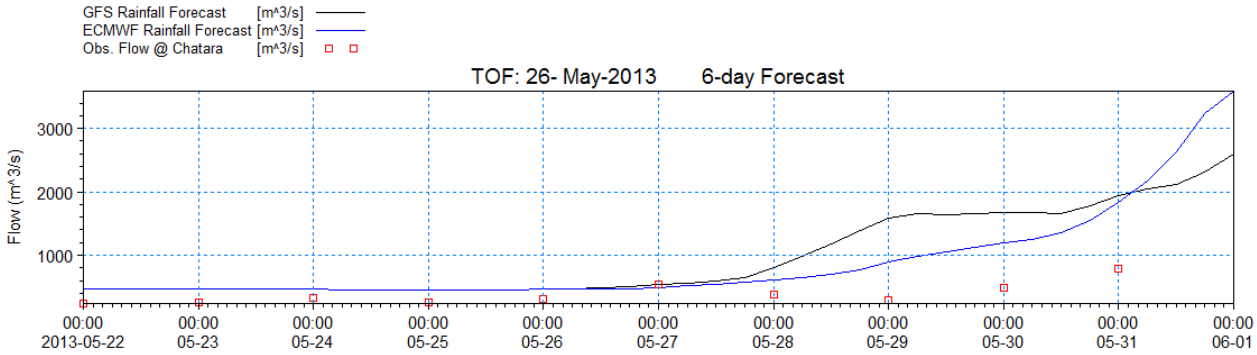

This case was taken in the latest pre- monsoon time period (May 2013). The purpose of taking this time period is to assess the accuracy of the FF model for recent pre monsoon flow. Data training in hindcast period is over estimated. Flood forecasting shows good prediction after 1-day for both GFS and ECMWF rainfall forecast data. Forecasting becomes unacceptable after 2 days.

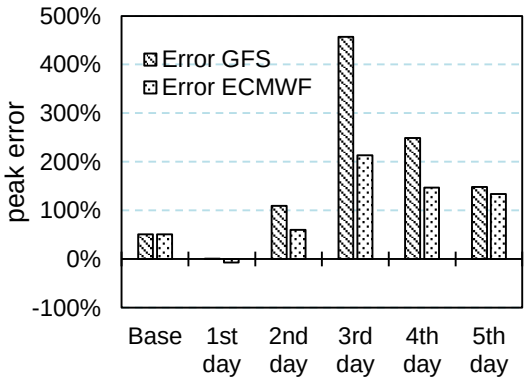

5.5.4 Case-4: Recent low flow

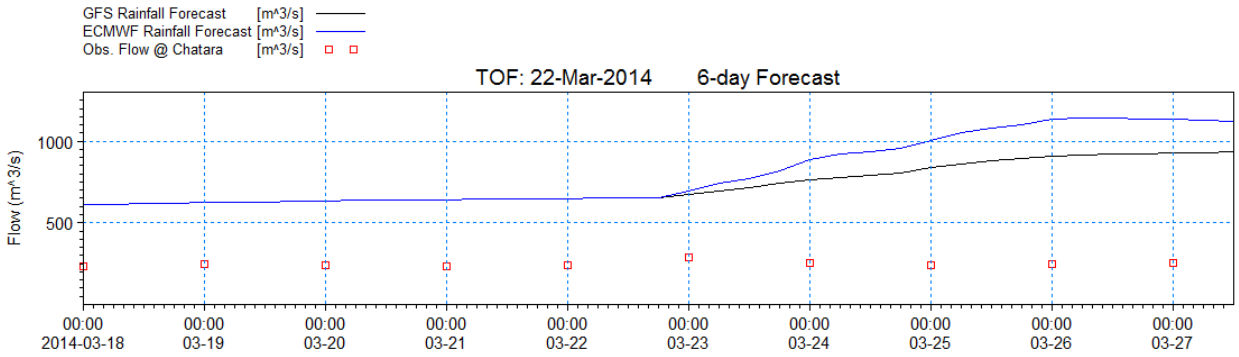

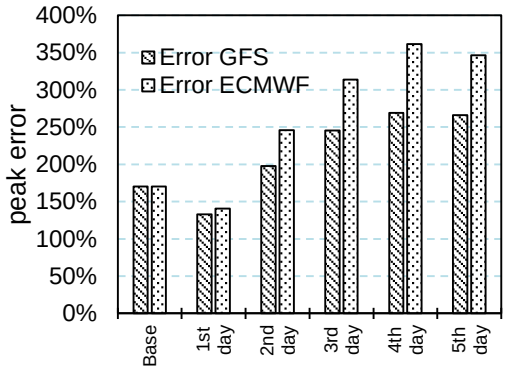

This case was taken in the latest time period (March 2014). The purpose of taking this time period is to assess the accuracy of the FF model for recent flow and also to check the data assimilation with recent data. As the base NAM and HD model is over estimated for low flow, FF model also shows similar behavior. Forecasting is appeared as overestimated from the beginning and the amount of overestimation increases as the number of forecasting day increases.

CHAPTER 6
SUMMARY, CONCLUSIONS AND RECOMMENDATIONS

6.1 SUMMARY

Recent statistics exhibits that the frequency of flood occurrence is increasing due to changed climatic condition, human intervention and different anthropogenic activities. The Koshi River is one of the major tributaries of the Ganges River. This river is originated from Himalayan mountain range. Every year this river carries a tremendous amount of water and sediment load and before joining into the Ganges River it creates flood in Bihar India. Flood forecasting in Koshi River will help the downstream areas to develop a state of the art flood warning system. Flood forecasting model development requires different hydro-meteorological information. As upstream of the Koshi River basin is in inaccessible Himalayan region, data procurement appears problematic. After ground truthing of acquired remote sensed satellite data, it can be used to improve flood mitigation strategies.

Koshi river basin can divided into trans-mountain, central mountain, eastern mountain, eastern hill and central hill regions and each region has separate climatic characteristics. The Koshi or Saptakoshi River have few tributaries. Among them Tamor Koshi originating from Mt. Kanchenjunga in the east, Arun Koshi from Mt. Everest in Tibet and Sun Koshi from Mt. Gosainthan farther west. Due to high sediment load, the Koshi River has a history of course shift. This river basin can be demarcated into 5 elevation zone. In the lower elevation terai and swalik zone, tropical climate prevail where high elevation alpine and snowline zone exhibits Arctic climate. This arctic condition cause glacier development in that region.

Hydro-meteorological data is required to develop hydrological and hydro dynamic model. Historical observed data was acquired from DHM. For remote flow estimation technique, AMSR-E microwave data, LANDSAT data was acquired from NASA and JAXA websites and processed at the same time. ASTER 30 m DEM was used for catchment delineation and cross section extraction. Rainfall forecast data was acquired from GFS model of NCEP and model of ECMWF. Data was processed accordingly for GFS and ECMWF rainfall data.

Real time flow estimation is an important step for flood forecasting model. This improves the forecast quality. A technique was developed using AMSR-E microwave image. Microwave image have an advantage that it is not affected by cloud interference though its resolution is coarse. This technique develops a relation between M/C ration and observed flow. M/C ration is the ratio of measuring wet pixel with calibrated dry pixel. This relation provides a rating curve of M/C ratio or flood signal and discharge. This rating curve equation is used for flow simulation. But this technique exhibits about 75% correlation between simulated and observed flow with 0.0092 m/km ground slope or lower. Above this slope this microwave AMSR-E approach technique does not show acceptable correlation, because that region is denoted as mountainous region. Rivers in mountainous region are comparatively narrow and there is no flood plain. The principle of this technique is to estimate the flow with respect to increment of moisture content in that pixel. In plain area, water stage spread

over the flood plain with the increment of discharge. But in the mountainous region, river width does not change significantly with discharge, which makes microwave AMSR-E based remote flow estimation technique invalid.

The principle of water surface reflectance approach for remote flow estimation is the attenuation attribute of spectrum in water. Lower wavelength of blue band penetrated deeper and less absorbed by water whereas higher wavelength of red band penetrates less than blue or similar lower wavelength band and also absorbed by water. This attenuation attribute can be correlate with observed flow. For this technique high resolution imagery is required. LANDSAT 30 m images was used to estimate flow. LANDSAT images are not available in daily basis and also interfered by cloud cover in monsoon. For model training and testing, few images were procured. Simulated data shows acceptable error with observed flow. Comparison among observed flow, estimated flow and flow from NAM model was performed and results shows acceptable correlation.

For hydrologic model rainfall data was acquired from TRMM satellite and from Aphrodite website. Aphrodite is observed rainfall which is available in gridded format upto year 2007. TRMM rainfall shows less correlation with same location observed rainfall information. To overcome this problem, TRMM rainfall was corrected using Aphrodite data as base. Model was run using both rainfall separately. Temperature and evaporation data was acquired from Aphrodite website upto year 2007. A relationship was developed between temperature and evaporation to estimate the evaporation for the year after 2007. In the case of temperature, a correlation was developed between MODIS LST and adjacent air temperature. Appropriate correction was done to fit the temperature with temperature change trend. After error analysis it was observed that model using Aphrodite rainfall data is more appropriate for flood forecasting.

For hydrodynamic model, discharge data was acquired from DHM, but no water level data was available. Cross section data was extracted from DEM. After calibration and validation, it was observed that there was not much difference between NAM model outcome and HD model outcome.

Using developed flood forecasting model, flood forecast was analyzed at Chatara station for several cases. Due to unavailability of observed water level data, only flow forecasting is possible. As the model was calibrated considering that the peak flow should be not be under estimated, this leads to an overestimated low flow period. This is also reflected in the flow forecasting for low flow period. For the flow forecasting in the monsoon period, forecasting depends on rainfall forecasting. Using observed rainfall as rainfall forecast, shows perfect outcome. But using GFS or ECMWF rainfall forecast, flow forecasting exhibits random results. Using pre-monsoon and monsoon flow to test the FF model shows that, flow forecast is in acceptable limit upto 2-4 day. After 4 days flow forecast has high error. This FF model is has capability to work with recent dataset and forecast in real time.

6.2 CONCLUSIONS

- Passive microwave approach technique for remote flow estimation is satisfactory for flood plain region, but for mountainous region or where flood plain is not significant, this technique does not work.
- Water surface reflectance approach for flow estimation is appropriate technique for mountainous region, but resolution imagery is required to improve correlation. As LANDSAT data is not available in daily basis, time series generation is not possible using this technique.
- It was planned that estimated flow using remote sensing will be used for real time flow updating. As TS generation is not possible using water surface reflectance approach, flood forecasting model has to perform without real time updating.
- TRMM rainfall does not show significant sensitivity with catchment runoff. Correction of TRMM rainfall according to observed Aphrodite rainfall data need to be done to use in the model.
- Hydrological model using Aphrodite rainfall data appears more appropriate for flood forecasting.
- Hydro-dynamic model results does not show any significant result deviation with respect to hydrological model, as no other outer catchment contributes inflow into this basin area.
- Monsoon flow forecasting shows high error after 2-4 days forecast using either GFS or ECMWF rainfall forecast data.
- FF model is ready to use in real time with recent dataset.

6.3 RECOMMENDATIONS

6.3.1 Recommendations based on the study results

Following recommendations are made based on research study findings,

- FF model can be calibrated using water level and water level forecast could be available.
- FF model can be developed using observed hydro-meteorological data rather than satellite estimated data.

6.3.2 Recommendations for further research

Following recommendations are made for further research,

- When LANDSAT constellation is available, it is assumed that image will be available more frequently then now. Water surface reflectance approach for flow estimation will be useful for flow TS generation.
- FF model can be developed using real time telemetric flow assimilation system. Forecast quality will be more accurate.

REFERENCES

Bajracharya, S. R., & Mool, P. (2009). Glaciers, glacial lakes and glacial lake outburst floods in the Mount Everest region. *Annals of Glaciology*, (50 (53)), 81–86.

Bapalu, G. V., & Sinha, R. (2005). GIS in Flood Hazard Mapping: a case study of Kosi River Basin, India.

Bharati, L., Gurung, P., & Jayakody, P. (2012). Hydrologic Characterization of the Koshi Basin and the Impact of Climate Change. *Hydro Nepal: Journal of Water, Energy and Environment*, *11*(1). doi:10.3126/hn.v11i1.7198

Birkinshaw, S. J., O'Donnell, G. M., Moore, P., Kilsby, C. G., Fowler, H. J., & Berry, P. A. M. (2010). Using satellite altimetry data to augment flow estimation techniques on the Mekong River. *Hydrological Processes*, *24*(26), 3811–3825. doi:10.1002/hyp.7811

Bjerklie, D. M., Moller, D., Smith, L. C., & Dingman, S. L. (2005). Estimating discharge in rivers using remotely sensed hydraulic information. *Journal of Hydrology*, *309*(1–4), 191–209. doi:10.1016/j.jhydrol.2004.11.022

Brakenridge, G. R., Cohen, S., Kettner, A. J., De Groeve, T., Nghiem, S. V., Syvitski, J. P. M., & Fekete, B. M. (2012). Calibration of satellite measurements of river discharge using a global hydrology model. *Journal of Hydrology*, *475*, 123–136. doi:10.1016/j.jhydrol.2012.09.035

Brakenridge, G. R., Nghiem, S. V., Anderson, E., & Chien, S. (2005). Space-based measurement of river runoff. *Transactions American Geophysical Union*, *86*(19), 185–188. doi:10.1029/2005EO190001

Brakenridge, G. R., Nghiem, S. V., Anderson, E., & Mic, R. (2007). Orbital microwave measurement of river discharge and ice status: Microwave Measurement of river discharge. *Water Resources Research*, *43*(4), n/a–n/a. doi:10.1029/2006WR005238

Cashion, J., Lakshmi, V., Bosch, D., & Jackson, T. J. (2005). Microwave remote sensing of soil moisture: evaluation of the TRMM microwave imager (TMI) satellite for the Little River Watershed Tifton, Georgia. *Journal of Hydrology*, *307*(1–4), 242–253. doi:10.1016/j.jhydrol.2004.10.019

Chakraborty, T., Kar, R., Ghosh, P., & Basu, S. (2010). Kosi megafan: Historical records, geomorphology and the recent avulsion of the Kosi River. *Quaternary International*, *227*(2), 143–160. doi:10.1016/j.quaint.2009.12.002

Chang, L. C. (1997). Satellite remote sensing of river inundation area, stage, and discharge: a review. *Hydrological Processes*, *11*(10), 1427–1439. doi:10.1002/(SICI)1099-1085(199708)11:10<1427::AID-HYP473>3.0.CO;2-S

Chang, L. C., & Pavelsky, T. M. (2008). Estimation of river discharge, propagation speed, and hydraulic geometry from space: Lena River, Siberia. *Water Resources Research*, *44*(3), n/a–n/a. doi:10.1029/2007WR006133

Chang, L. C., Shen, H. Y., Wang, Y. F., Huang, J. Y., & Lin, Y. T. (2010). Clustering-based hybrid inundation model for forecasting flood inundation depths. *Journal of Hydrology*, *385*(1–4), 257–268. doi:10.1016/j.jhydrol.2010.02.028

Chen, H., Yang, D., Hong, Y., Gourley, J. J., & Zhang, Y. (2013). Hydrological data assimilation with the Ensemble Square-Root-Filter: Use of streamflow observations to

update model states for real-time flash flood forecasting. *Advances in Water Resources*, *59*, 209–220. doi:10.1016/j.advwatres.2013.06.010

Chow, V. T. (1959). *Open-channel hydraulics*. McGraw-Hill.

Dahal, R. K., & Hasegawa, S. (2008). Representative rainfall thresholds for landslides in the Nepal Himalaya. *Geomorphology*, *100*(3–4), 429–443. doi:10.1016/j.geomorph.2008.01.014

De Groeve, T. (2010). Flood monitoring and mapping using passive microwave remote sensing in Namibia. *Geomatics, Natural Hazards and Risk*, *1*(1), 19–35. doi:10.1080/19475701003648085

De Groeve, T., Kugler, Z., & Brakenridge, G. R. (2007). Near Real Time Flood Alerting for the Global Disaster Alert and Coordination System. Presented at the Intelligent Human Computer Systems for Crisis Response and Management, Delft, Netherlands.

Devkota, L., Crosato, A., & Giri, S. (2012). Effect of the barrage and embankments on flooding and channel avulsion case study Koshi River, Nepal. *A Journal of Rural Infrastructure Development, Society of Engineers' for Rural Development, Nepal (SERDeN)*, *3*(3), 124–132.

DHI. (2012). *A Modelling System for Rivers and Channels- Reference Manual of MIKE 11* (7th Edition.).

Durand, M., Anderson, E., Alsdorf, D. E., & Trigg, M. (2010). Estimating River Depth From Remote Sensing Swath Interferometry Measurements of River Height, Slope, and Width. *IEEE Journal of Selected Topics in Applied Earth Observations and Remote Sensing*, *3*(1), 20–31. doi:10.1109/JSTARS.2009.2033453

Fakhruddin, S. H. M., & Hassan, A. (2003). Discharge Prediction Method using Remote Sensing and Hydrological Data. *Center for Environmental and Geographic Information Services (CEGIS), Bangladesh*.

Firat, M. (2008). Comparison of Artificial Intelligence Techniques for river flow forecasting. *Hydrology and Earth System Sciences*, *12*(1), 123–139. doi:10.5194/hess-12-123-2008

Gordon, H. R., Clark, D. K., Brown, J. W., Brown, O. B., Evans, R. H., & Broenkow, W. W. (1983). Phytoplankton pigment concentrations in the Middle Atlantic Bight: comparison of ship determinations and CZCS estimates. *Applied Optics*, *22*(1), 20. doi:10.1364/AO.22.000020

Hirpa, F. A., Hopson, T. M., De Groeve, T., Brakenridge, G. R., Gebremichael, M., & Restrepo, P. J. (2013). Upstream satellite remote sensing for river discharge forecasting: Application to major rivers in South Asia. *Remote Sensing of Environment*, *131*, 140–151. doi:10.1016/j.rse.2012.11.013

Hong, S. (2010). Detection of small-scale roughness and refractive index of sea ice in passive satellite microwave remote sensing. *Remote Sensing of Environment*, *114*(5), 1136–1140. doi:10.1016/j.rse.2009.12.015

Hossain, F., Maswood, M., iddique-E-Akbor, A. H., & Yigzaw, W. (2013). Can a Radar Altimetry Satellite Deliver on the Promise of an Operational and Real-Time Transboundary Flood Forecasting System for Flood-prone Bangladesh? *Water Resources Research*.

Ines, A. V. M., & Hansen, J. W. (2006). Bias correction of daily GCM rainfall for crop simulation studies. *Agricultural and Forest Meteorology*, *138*(1-4), 44–53. doi:10.1016/j.agrformet.2006.03.009

Jain, S. S. K., Agarwal, P. K., & Singh, V. V. P. (2007). *Hydrology and Water Resources of India*. Springer.

Li, D., Durand, M., & Margulis, S. A. (2012). Potential for hydrologic characterization of deep mountain snowpack via passive microwave remote sensing in the Kern River basin, Sierra Nevada, USA. *Remote Sensing of Environment*, *125*, 34–48. doi:10.1016/j.rse.2012.06.027

Looper, J. P., & Vieux, B. E. (2012). An assessment of distributed flash flood forecasting accuracy using radar and rain gauge input for a physics-based distributed hydrologic model. *Journal of Hydrology*, *412–413*, 114–132. doi:10.1016/j.jhydrol.2011.05.046

Lu, H., Koike, T., Yang, K., Hu, Z., Xu, X., & Rasmy, M. (2012). Improving land surface soil moisture and energy flux simulations over the Tibetan plateau by the assimilation of the microwave remote sensing data and the GCM output into a land surface model. *International Journal of Applied Earth Observation and Geoinformation*, *17*, 43–54. doi:10.1016/j.jag.2011.09.006

Majozi, N. P. (2011, February). *Remote Sensing of Euphotic depth in Lake Naivasha*. University of Twente, Netherlands.

Meena, R. S. (2012, October). *Simulation of Runoff and Flood Inundation in Koshi River Basin Using Hydrological Models, ANN, Remote Sensing And GIS*. National Institute of Technology, Rourkela.

Mool, P. (2002). *Inventory of glaciers, glacial lakes and glacial lake outburst floods monitoring and early warning systems in the Hindu Kush-Himalayan Region, Bhutan*. Kathmandu, Nepal: International Centre for Integrated Mountain Development, Mountain Environment and Natural Resources' Information Systems.

Mukerji, A., Chatterjee, C., & Raghuwanshi, N. S. (2009). Flood Forecasting Using ANN, Neuro-Fuzzy, and Neuro-GA Models. *Journal of Hydrologic Engineering*.

Nepal, S. (2012, July 4). *Evaluating Upstream Downstream Linkages of Hydrological Dynamics in the Himalayan Region*. Friedrich-Schiller-University Jena, Jena. Retrieved from http://lib.icimod.org/record/27091

Ninsawat, S., Yamamotoa, H., Nakamura, R., Kamei, A., Kato, S. X., & Tsuchida, S. (2010). Development of OGC Framework For Estimating Air Temperature From MODIS LST And Sensor Network. Presented at the WebMGS 2010 1st International Workshop on Pervasive Web Mapping, Geoprocessing and Services, Como, Italy.

Nkemdirim, L. C. (1991). Chinooks and winter evaporation. *Theoretical and Applied Climatology*, *43*(3), 129–136. doi:10.1007/BF00867470

Panda, R. K., Pramanik, N., & Bala, B. (2010). Simulation of river stage using artificial neural network and MIKE 11 hydrodynamic model. *Computers & Geosciences*, *36*(6), 735–745. doi:10.1016/j.cageo.2009.07.012

Papa, F., Durand, F., Rossow, W. B., Rahman, A., & Bala, S. K. (2010). Satellite altimeter-derived monthly discharge of the Ganga-Brahmaputra River and its seasonal to interannual variations from 1993 to 2008. *Journal of Geophysical Research*, *115*(C12). doi:10.1029/2009JC006075

Ramachandran, B., Justice, C. O., & Abrams, M. J. (2010). *Land Remote Sensing and Global Environmental Change: NASA's Earth Observing System and the Science of ASTER and MODIS*. Springer.

Rossa, A. M., Laudanna Del Guerra, F., Borga, M., Zanon, F., Settin, T., & Leuenberger, D. (2010). Radar-driven high-resolution hydro-meteorological forecasts of the 26 September 2007 Venice flash flood. *Journal of Hydrology*, *394*(1–2), 230–244. doi:10.1016/j.jhydrol.2010.08.035

Shah-Newaz, S. M., & Magumdar, T. K. (2011). Flood Forecasting in Bagmati Basin using MIKE 11 model, Rainfall Forecast Assimilation and Real Time Inundation Mapping. Regional Integrated Multi-hazard Early Warning System for Africa and Asia (RIMES).

Shrestha, A. B., Wake, C. P., Mayewski, P. A., & Dibb, J. E. (1999). Maximum Temperature Trends in the Himalaya and Its Vicinity: An Analysis Based on Temperature Records from Nepal for the Period 1971–94. *Journal of Climate*, *12*(9), 2775–2786. doi:10.1175/1520-0442(1999)012<2775:MTTITH>2.0.CO;2

Stronska, K., Kitowski, K., & Jorgensen, G. (1999). MIKE 11 as Flood Management and Flood Forecasting Tool for the Odra River, Poland. In *3rd DHI Software Conf.* Helsingor.

Stumpf, R. P., Holderied, K., & Sinclair, M. (2003). Determination of water depth with high-resolution satellite imagery over variable bottom types. *Limnology and Oceanography*, *48*(1_part_2), 547–556. doi:10.4319/lo.2003.48.1_part_2.0547

Sun, Q., & Lu, D. (2005). The sensitivity analysis of microwave radiometer's brightness temperature and geophysical parameters (Vol. 5832, pp. 609–614). Presented at the Society of Photo-Optical Instrumentation Engineers (SPIE) Conference Series. doi:10.1117/12.619873

Tiwari, M. K., & Chatterjee, C. (2010). Uncertainty assessment and ensemble flood forecasting using bootstrap based artificial neural networks (BANNs). *Journal of Hydrology*, *382*(1–4), 20–33. doi:10.1016/j.jhydrol.2009.12.013

Ueno, K., Toyotsu, K., Bertolani, L., & Tartari, G. (2008). Stepwise Onset of Monsoon Weather Observed in the Nepal Himalaya. *Monthly Weather Review*, *136*(7), 2507–2522. doi:10.1175/2007MWR2298.1

Upreti, B. N. (1999). An overview of the stratigraphy and tectonics of the Nepal Himalaya. *Journal of Asian Earth Sciences*, (17), 577–606.

Vermote, E. F., & Vermeulen, A. (1999). *{Atmospheric correction algorithm: spectral reflectances (MOD09). Algorithm Technical Background Document (ATBD)}*. Retrieved from http://modis.gsfc.nasa.gov/data/atbd/atbd_mod08.pdf

Wardah, T., Fakhruddin, S. H. M., Bardossy, A., & Maznorizan, M. (2008). Use of geostationary meteorological satellite images in convective rain estimation for flash-flood forecasting. *Journal of Hydrology*, *356*(3–4), 283–298. doi:10.1016/j.jhydrol.2008.04.015

WMO. (2011). *Manual on flood forecasting and warning*. Geneva: World Meteorological Organization.

Zhang, A., & Jia, G. (2013). Monitoring meteorological drought in semiarid regions using multi-sensor microwave remote sensing data. *Remote Sensing of Environment*, *134*, 12–23. doi:10.1016/j.rse.2013.02.023

APPENDIX-A

Flood Signal Generation Tool

GIS MODEL:

```
# Import arcpy module
import arcpy
# Check out any necessary licenses
arcpy.CheckOutExtension("spatial")
# Load required toolboxes
arcpy.ImportToolbox("Model Functions")
# Script arguments
Input_Raster_Folder = arcpy.GetParameterAsText(0)
Grid = arcpy.GetParameterAsText(1)
if Grid == '#' or not Grid:
    Grid = "D:\\GIS\\Tool\\Chatara\\grid_mountain.shp" # provide a default value if unspecified
Study_Location = arcpy.GetParameterAsText(2)
if Study_Location == '#' or not Study_Location:
    Study_Location = "'87.092 26.751'" # provide a default value if unspecified
Output_Location = arcpy.GetParameterAsText(3)
if Output_Location == '#' or not Output_Location:
    Output_Location = "D:\\GIS\\Tool\\Chatara\\FS" # provide a default value if unspecified
# Local variables:
Raster_Grid = Grid
mcell = Raster_Grid
cCell__2_ = mcell
cCell__4_ = cCell__2_
cCell__5_ = cCell__4_
cCell__3_ = cCell__5_
cCell__6_ = cCell__3_
cCell__7_ = cCell__6_
cCell__8_ = cCell__7_
Flood_Signal = cCell__8_
cCell = Raster_Grid
Input_Raster = Input_Raster_Folder
Name = Input_Raster_Folder
# Process: Iterate Rasters
arcpy.IterateRasters_mb(Input_Raster_Folder, "", "", "NOT_RECURSIVE")
# Process: Raster Grid Extraction
arcpy.gp.ExtractByMask_sa(Input_Raster, Grid, Raster_Grid)
# Process: Calibration Point Extraction
arcpy.Statistics_analysis(Raster_Grid, cCell, "VALUE MAX", "")
# Process: Focal Point Extraction
arcpy.gp.ExtractByPoints_sa(Raster_Grid, Study_Location, mcell, "INSIDE")
# Process: Join Field
arcpy.JoinField_management(cCell, "ROWID", mcell, "Rowid", "")
# Process: Add Field
arcpy.AddField_management(cCell__2_, "C", "DOUBLE", "20", "8", "", "", "NULLABLE",
"NON_REQUIRED", "")
# Process: Add Field (2)
arcpy.AddField_management(cCell__4_, "M", "DOUBLE", "20", "8", "", "", "NULLABLE",
"NON_REQUIRED", "")
# Process: Add Field (3)
```

```
arcpy.AddField_management(cCell__5_, "FS", "DOUBLE", "20", "8", "", "", "NULLABLE",
"NON_REQUIRED", "")
# Process: Calculate Field
arcpy.CalculateField_management(cCell__3_, "C", "[MAX_VALUE]/100+100", "VB", "")
# Process: Calculate Field (2)
arcpy.CalculateField_management(cCell__6_, "M", "[VALUE]/100+100", "VB", "")
# Process: Calculate Field (3)
arcpy.CalculateField_management(cCell__7_, "FS", "[M]/ [C]", "VB", "")
# Process: Flood Signal Generation
arcpy.TableToTable_conversion(cCell__8_, Output_Location, Name, "", "C \"Calibration (Tb)\" true
true false 8 Double 0 0 ,First,#,D:\\GIS\\Tool\\Chatara\\cCell,C,-1,-1;M \"Measured\" true true false 8
Double 0 0 ,First,#,D:\\GIS\\Tool\\Chatara\\cCell,M,-1,-1;FS \"Flood Signal\" true true false 8 Double
0 0 ,First,#,D:\\GIS\\Tool\\Chatara\\cCell,FS,-1,-1", "")
```

VBA for Excel

```
Sub dbfMerger()
Dim bookList As Workbook
Dim mergeObj As Object, dirObj As Object, files As Object, everyObj As Object
Application.ScreenUpdating = False
Set mergeObj = CreateObject("Scripting.FileSystemObject")
Set dirObj = mergeObj.Getfolder("Folder Location")
Set fileObj = dirObj.files
For Each everyObj In fileObj
Set bookList = Workbooks.Open(everyObj)
Range("A2:C2").Copy
ThisWorkbook.Worksheets(1).Activate
Range("A65536").End(xlUp).Offset(1, 0).PasteSpecial
Application.CutCopyMode = False
bookList.Close
Next
End Sub
```

Water Surface Reflectance Extraction Tool

GIS Model

```
# Import arcpy module
import arcpy
# Check out any necessary licenses
arcpy.CheckOutExtension("spatial")
# Script arguments
Blue_Band = arcpy.GetParameterAsText(0)
Green_Band = arcpy.GetParameterAsText(1)
NIR_Band = arcpy.GetParameterAsText(2)
Grid_Point = arcpy.GetParameterAsText(3)
elevation_angel = arcpy.GetParameterAsText(4)
d = arcpy.GetParameterAsText(5)
rad_mult_blue = arcpy.GetParameterAsText(6)
rad_mult_green = arcpy.GetParameterAsText(7)
rad_mult_NIR = arcpy.GetParameterAsText(8)
```

```
rad_add_blue = arcpy.GetParameterAsText(9)
rad_add_green = arcpy.GetParameterAsText(10)
rad_add_NIR = arcpy.GetParameterAsText(11)
esun_blue = arcpy.GetParameterAsText(12)
if esun_blue == '#' or not esun_blue:
    esun_blue = "2067" # provide a default value if unspecified
esun_green = arcpy.GetParameterAsText(13)
if esun_green == '#' or not esun_green:
    esun_green = "1893" # provide a default value if unspecified
esun_NIR = arcpy.GetParameterAsText(14)
if esun_NIR == '#' or not esun_NIR:
    esun_NIR = "972.6" # provide a default value if unspecified
# Local variables:
DN_Blue = Blue_Band
Radiance_Output = DN_Blue
Radiance = Radiance_Output
Zenith_Output = Radiance
Zenith = Zenith_Output
Reflectance_Output = Zenith
Blue_Reflectance = Reflectance_Output
output__3_ = Blue_Reflectance
DN_Green = Green_Band
Radiance_Output__2_ = DN_Green
Radiance__2_ = Radiance_Output__2_
Zenith_Output__2_ = Radiance__2_
Zenith__2_ = Zenith_Output__2_
Reflectance_Output__2_ = Zenith__2_
Green_Reflectance = Reflectance_Output__2_
DN_NIR = Grid_Point
Radiance_Output__3_ = DN_NIR
Radiance__3_ = Radiance_Output__3_
Zenith_Output__3_ = Radiance__3_
Zenith__3_ = Zenith_Output__3_
Reflectance_Output__3_ = Zenith__3_
NIR_Reflectance = Reflectance_Output__3_
output = "E:\\GIS\\Tool_Reflectance\\output"
# Process: Extraction Blue
arcpy.gp.ExtractValuesToPoints_sa(Grid_Point, Blue_Band, DN_Blue, "NONE", "VALUE_ONLY")
# Process: Radiance Field
arcpy.AddField_management(DN_Blue, "radiance", "DOUBLE", "", "", "", "", "NULLABLE",
"NON_REQUIRED", "")
# Process: Calculate Radiance
arcpy.CalculateField_management(Radiance_Output, "radiance",
"[RASTERVALU]*%rad_mult_blue%+%rad_add_blue%", "VB", "")
# Process: Zenith Field
arcpy.AddField_management(Radiance, "cos", "DOUBLE", "", "", "", "", "NULLABLE",
"NON_REQUIRED", "")
# Process: Calculate Zenith
```

```
arcpy.CalculateField_management(Zenith_Output, "cos", "Cos (0.0174532925*(90 - %elevation_angel% ))", "VB", "")
# Process: Reflectance Field
arcpy.AddField_management(Zenith, "reflectance", "DOUBLE", "", "", "", "", "NULLABLE", "NON_REQUIRED", "")
# Process: Calculate Reflectance
arcpy.CalculateField_management(Reflectance_Output, "reflectance", "(3.1415926* [radiance] *%d%*%d%)/(%esun_blue%* [cos] )", "VB", "")
# Process: Extraction Green
arcpy.gp.ExtractValuesToPoints_sa(Grid_Point, Green_Band, DN_Green, "NONE", "VALUE_ONLY")
# Process: Radiance Field (2)
arcpy.AddField_management(DN_Green, "radiance", "DOUBLE", "", "", "", "", "NULLABLE", "NON_REQUIRED", "")
# Process: Calculate Radiance (2)
arcpy.CalculateField_management(Radiance_Output__2_, "radiance", "[RASTERVALU]*%rad_mult_green%+%rad_add_green%", "VB", "")
# Process: Zenith Field (2)
arcpy.AddField_management(Radiance__2_, "cos", "DOUBLE", "", "", "", "", "NULLABLE", "NON_REQUIRED", "")
# Process: Calculate Zenith (2)
arcpy.CalculateField_management(Zenith_Output__2_, "cos", "Cos (0.0174532925*(90 - %elevation_angel% ))", "VB", "")
# Process: Reflectance Field (2)
arcpy.AddField_management(Zenith__2_, "reflectance", "DOUBLE", "", "", "", "", "NULLABLE", "NON_REQUIRED", "")
# Process: Calculate Reflectance (2)
arcpy.CalculateField_management(Reflectance_Output__2_, "reflectance", "(3.1415926* [radiance] *%d%*%d%)/(%esun_green%* [cos] )", "VB", "")
# Process: Extraction NIR
arcpy.gp.ExtractValuesToPoints_sa(Grid_Point, NIR_Band, DN_NIR, "NONE", "VALUE_ONLY")
# Process: Radiance Field (3)
arcpy.AddField_management(DN_NIR, "radiance", "DOUBLE", "", "", "", "", "NULLABLE", "NON_REQUIRED", "")
# Process: Calculate Radiance (3)
arcpy.CalculateField_management(Radiance_Output__3_, "radiance", "[RASTERVALU]*%rad_mult_NIR%+%rad_add_NIR%", "VB", "")
# Process: Zenith Field (3)
arcpy.AddField_management(Radiance__3_, "cos", "DOUBLE", "", "", "", "", "NULLABLE", "NON_REQUIRED", "")
# Process: Calculate Zenith (3)
arcpy.CalculateField_management(Zenith_Output__3_, "cos", "Cos (0.0174532925*(90 - %elevation_angel% ))", "VB", "")
# Process: Reflectance Field (3)
arcpy.AddField_management(Zenith__3_, "reflectance", "DOUBLE", "", "", "", "", "NULLABLE", "NON_REQUIRED", "")
# Process: Calculate Reflectance (3)
```

```
arcpy.CalculateField_management(Reflectance_Output__3_, "reflectance", "(3.1415926* [radiance] *%d%*%d%)/(%esun_NIR%* [cos] )", "VB", "")
# Process: Table to dBASE (multiple)
arcpy.TableToDBASE_conversion("E:\\GIS\\Tool_Reflectance\\reflectance.gdb\\extr_blue;E:\\GIS\\Tool_Reflectance\\reflectance.gdb\\extr_green;E:\\GIS\\Tool_Reflectance\\reflectance.gdb\\extr_NIR", output)
```

TRMM Rainfall Extraction Tool

GIS Model

```
# Import arcpy module
import arcpy
# Check out any necessary licenses
arcpy.CheckOutExtension("spatial")
# Load required toolboxes
arcpy.ImportToolbox("Model Functions")
# Script arguments
NC_File_Location = arcpy.GetParameterAsText(0)
if NC_File_Location == '#' or not NC_File_Location:
    NC_File_Location = "E:\\GIS\\Tool_RF\\TRMM\\test" # provide a default value if unspecified
Grid = arcpy.GetParameterAsText(1)
if Grid == '#' or not Grid:
    Grid = "E:\\GIS\\Tool_RF\\shp\\raster_76.shp" # provide a default value if unspecified
Output_Folder = arcpy.GetParameterAsText(2)
if Output_Folder == '#' or not Output_Folder:
    Output_Folder = "E:\\GIS\\Tool_RF\\table" # provide a default value if unspecified
# Local variables:
File = NC_File_Location
Precepititation_Raster = File
temp_shp = Precepititation_Raster
Output_dbf = temp_shp
Name = NC_File_Location
# Process: Iterate Files
arcpy.IterateFiles_mb(NC_File_Location, "", "", "NOT_RECURSIVE")
# Process: Make NetCDF Raster Layer
arcpy.MakeNetCDFRasterLayer_md(File, "precipitation", "lon", "lat", Precepititation_Raster, "", "", "BY_VALUE")
# Process: Extract Values to Points
arcpy.gp.ExtractValuesToPoints_sa(Grid, Precepititation_Raster, temp_shp, "NONE", "VALUE_ONLY")
# Process: Table to Table
arcpy.TableToTable_conversion(temp_shp, Output_Folder, Name, "", "Lat \"Lat\" true true false 13 Double 3 12 ,First,#,E:\\GIS\\Tool_RF\\temp\\temp.shp,Lat,-1,-1;Long \"Long\" true true false 13 Double 3 12 ,First,#,E:\\GIS\\Tool_RF\\temp\\temp.shp,Long,-1,-1;RASTERVALU \"RASTERVALU\" true true false 19 Double 8 18 ,First,#,E:\\GIS\\Tool_RF\\temp\\temp.shp,RASTERVALU,-1,-1", "")
```

VBA for Excel

```
Sub dbfMerger()
Dim bookList As Workbook
Dim mergeObj As Object, dirObj As Object, files As Object, everyObj As Object
```

```
Application.ScreenUpdating = False
Set mergeObj = CreateObject("Scripting.FileSystemObject")
Set dirObj = mergeObj.Getfolder("E:\GIS\Tool_RF\table")
Set fileObj = dirObj.files
For Each everyObj In fileObj
Set bookList = Workbooks.Open(everyObj)
Range("C2:C77").Copy
ThisWorkbook.Worksheets(1).Activate
Range("XFD2").End(xlToLeft).Offset(0, 1).PasteSpecial
Application.CutCopyMode = False
bookList.Close
Next
End Sub
```

APPENDIX-B

Training Dataset of Chatara (2013-2014)

Date	Obs. Flow (m^3/s)	R_{blue}	R_{green}	R_{NIR}	Y	θ	R_r	$R_{w\ blue}$	$R_{w\ green}$	ln (nR_b)/ ln (nR_g)
14-01-14	335.8	0.131	0.105	0.058	1.470	136.540	1.054	-1.009	-1.035	0.989
27-11-13	520.1	0.121	0.102	0.051	1.890	132.580	1.007	-0.982	-1.001	0.991
11-11-13	751	0.114	0.100	0.035	1.020	133.810	1.021	-0.943	-0.957	0.993
26-10-13	1021.5	0.129	0.115	0.059	1.800	136.070	1.049	-1.027	-1.041	0.994
24-09-13	1617.9	0.120	0.110	0.086	1.796	141.910	1.118	-1.152	-1.163	0.996

*n = -10

Testing Dataset of Chatara (2001- 2007)

Date	Obs. Flow (m^3/s)	R_{blue}	R_{green}	R_{NIR}	Y	θ	$R_{w\ blue}$	$R_{w\ green}$	ln (nRb)/ ln (nRg)	Simulated Flow (m^3/s)	Error (%)
18-01-01	376	0.129	0.106	0.062	1.374	126.140	-0.886	-0.910	0.988	395.661	5.2%
19-02-01	347	0.134	0.118	0.080	1.279	132.830	-0.978	-0.993	0.993	736.223	112.2%
20-10-02	1120	0.120	0.106	0.069	1.054	136.490	-1.007	-1.021	0.994	922.286	17.7%
25-10-04	1080	0.116	0.102	0.061	0.858	134.340	-0.964	-0.978	0.994	874.575	19.0%
16-11-06	688	0.113	0.097	0.058	0.96	129.050	-0.908	-0.923	0.992	586.031	14.8%
18-10-07	1500	0.121	0.113	0.087	1.11	136.760	-1.032	-1.040	0.997	1776.946	18.5%
19-11-07	747	0.114	0.096	0.051	0.937	128.530	-0.893	-0.910	0.991	436.550	41.6%

*n = -10

Training Dataset of Mulghat (2001- 2007)

Date	Obs. Flow (m^3/s)	R_{blue}	R_{green}	R_{NIR}	Y	θ	R_r	$R_{w\ blue}$	$R_{w\ green}$	ln (nR_b)/ ln (nR_g)
18-01-01	61.5	0.122	0.096	0.083	1.374	126.140	0.931	-0.924	-0.950	0.988
19-02-01	50	0.122	0.099	0.093	1.279	132.830	1.010	-1.006	-1.029	0.990
20-10-02	284	0.120	0.107	0.075	1.054	136.490	1.054	-1.013	-1.026	0.994
16-11-06	106	0.116	0.096	0.069	0.960	129.050	0.965	-0.915	-0.934	0.991
18-10-07	263	0.122	0.113	0.085	1.110	136.760	1.057	-1.030	-1.038	0.997
19-11-07	74	0.116	0.096	0.068	0.937	128.530	0.958	-0.907	-0.927	0.990

*n =10

APPENDIX-C

Error Indicator of the Model using Corrected TRMM Rainfall

Number of days under estimated

	Turkeghat	Mulghat	Khurkot	Hampuachewar	Simle	Chatara
2001	12	29	20	23	7	4
2002	6	34	22	21	26	15
2003	10	25	26	20	11	25
2004	33	31	35	12	17	6
2005	7	28	36	31	2	3
2006	19	32	34	30	17	10
2007	21	33	34	30	9	3

Average under estimation

	Turkeghat	Mulghat	Khurkot	Hampuachewar	Simle	Chatara
2001	307.4	521.3	1265.9	651.9	382.6	110.8
2002	206.2	932.3	822.0	964.8	320.4	1045.2
2003	334.2	522.8	1234.8	571.4	335.7	1419.2
2004	239.2	443.7	1105.7	368.7	73.4	359.8
2005	281.3	246.4	1084.3	579.0	0.7	302.8
2006	230.7	385.7	1024.2	385.1	186.5	408.2
2007	343.7	315.3	1056.3	592.3	265.0	606.4

Error Indicator of the Model using Aphrodite Rainfall

Number of days under estimated

	Turkeghat	Mulghat	Khurkot	Hampuachewar	Simle	Chatara
2001	31	34	20	10	29	2
2002	18	33	6	5	30	3
2003	23	22	23	4	15	19
2004	33	28	34	0	13	0
2005	21	26	36	22	5	0
2006	29	28	34	11	24	4
2007	29	28	35	12	18	0

Average under estimation

	Turkeghat	Mulghat	Khurkot	Hampuachewar	Simle	Chatara
2001	506.6	476.1	740.1	329.7	418.0	404.8
2002	361.8	823.6	284.0	361.8	430.3	257.9
2003	353.0	538.8	653.5	417.0	462.8	915.8
2004	263.6	269.7	590.0	0.0	195.8	0.0
2005	233.6	270.3	872.5	378.8	168.0	0.0
2006	253.7	429.9	651.5	139.2	284.9	429.7
2007	439.0	224.9	721.2	350.0	258.3	0.0

APPENDIX-D

Correction Factors for Generated Temperature from LST

Catchment	Month Duration	Slope	Intercept
Arun-1	Jul-Oct	0.75	-4
	Nov-Jun	0.4	-6.5
Arun-2	May-Oct	1	-0.6226
	Nov-Apr	0.7	-0.6226
Tamor-1	Jun-Aug	1.4	-0.6226
	Oct-May	0.7	-0.6226
Tamor-2	May-Oct	0.9	-0.6226
	Nov-Apr	0.7	-0.6226
Likhu	Jun-Oct	1.5	1.5
	Nov-May	0.7	-0.6226
Indrawati	May-Oct	0.7	9.5
	Nov-Apr	0.7	-0.6226
Sun Koshi	May-Oct	0.9	-0.6226
	Nov-Apr	0.7	-0.6226
Dudh Koshi	Jul-Oct	1.5	3
	Nov-Jun	0.7	-0.6226
Tama Koshi	Jun-Oct	1.2	-2
	Nov-May	0.7	-0.6226
Bhote Koshi	May-Oct	0.5	5
	Nov-Apr	0.4	-0.6226